

# Simulating Transition Cells under the Transition Scale-Space Model in Spiking Neural Networks

Simen Storesund

May 11, 2024

## Acknowledgements

Completing a master's thesis is a test of independence, but that doesn't mean I could have done it by myself. I want to give huge thanks to Nicolai Waniek, my supervisor, for his continued interest and constructive comments throughout the project. I also want to thank him for allowing me to work on the TSS model, and for creating such an interesting model to start with. Next, I would like to thank Benjamin Dunn for cosupervising, providing constructive feedback, and to his group for letting me join their group meetings. Finally, thanks also goes to the Kavli Institute, both for the interesting work they do and for letting me have an office in their building.

# Contents

<b>1</b>	<b>Introduction</b>	<b>7</b>
1.1	Animal Navigation . . . . .	7
1.2	The Transition Scale-Space Model . . . . .	8
1.3	Spatial Cell Types in the Hippocampal Area . . . . .	10
1.3.1	Place cells . . . . .	10
1.3.2	Grid Cells . . . . .	12
1.3.3	Other Spatially Modulated Cells . . . . .	13
1.4	Existing Grid Cell Models . . . . .	14
1.5	Grid Cells as Potential Transition Neurons . . . . .	15
1.6	Thesis Goal . . . . .	16
<b>2</b>	<b>Methods</b>	<b>18</b>
2.1	Overall model design . . . . .	18
2.2	Considering BVC inputs . . . . .	19
2.3	Rectangularly spaced inputs . . . . .	21
2.4	Randomly spaced inputs . . . . .	22
2.5	Multi-Compartment Model . . . . .	23
2.6	Boundary vector cell inputs . . . . .	25
2.7	Other network models . . . . .	25
2.7.1	Rate coded inputs . . . . .	25
2.7.2	Linear Summation BVC model . . . . .	26
2.7.3	Linear Multi-compartment Models . . . . .	26
2.8	Simulation software . . . . .	27
2.9	Analysis . . . . .	27
<b>3</b>	<b>Results</b>	<b>30</b>
3.1	Defining Typical Parameters: a Standard Model . . . . .	30
3.2	Gridness scores in the different models . . . . .	33
3.3	Orientation and phase distribution . . . . .	37
3.4	Gridness spacing . . . . .	39
3.5	Temporal stability . . . . .	40
3.6	Boundary Vector Cell Inputs . . . . .	41
<b>4</b>	<b>Discussion</b>	<b>44</b>
4.1	What this model shows . . . . .	44
4.2	Biological plausibility of input distributions and multi-compartment models . . . . .	45
4.3	A word about parameters . . . . .	47
4.4	This model as an mEC grid cell model . . . . .	48
4.5	Comparison to existing grid cell models . . . . .	49
4.6	mECII as home to transition cells . . . . .	51

<b>5 Conclusion</b>	<b>52</b>
<b>A Appendix: A navigation model</b>	<b>59</b>
A.1 Introduction . . . . .	59
A.2 Methods . . . . .	59
A.3 Results . . . . .	60
A.4 Discussion . . . . .	63

## Summary

In the Transition Scale-Space model, entorhinal grid cells are interpreted as highly effective transition cells, responsible for accelerating retrieval of place-sequences during navigation. Previous simulations have shown that transition cells can develop hexagonal firing fields in populations of three cells, but not more. In this work, transition cell learning was simulated in spiking neural networks using theta-phase coded inputs and delayed lateral inhibition. This produced high levels of hexagonality in populations of 13 and 23 transition cells. There is also a suggestion on how boundary vector inputs can replace place inputs, using dendritic computation in a multicompartment model, which predicts that dendrites respond to single places in an even distribution across space. This is still a work in progress. There are also unanswered questions with regards to the structure of the population activity. Lastly, a pathfinding method compatible with TSS without backpropagation is presented. In sum, this is a work in favor of the biological plausibility of the TSS model, using computational resources available in biological neural networks.

## Sammendrag

Transition Scale-Spacemodellen forklarer gitterceller i entorhinal cortex som overgangsceller, som aksellererer produksjon av stedcellesekvenser ved navigasjon. I tidligere simuleringer utviklet overgangsceller heksagonalitet i nettverk på tre celler. I dette arbeidet ble overgangsceller simulert i nevrale nettverk i kontinuerlig tid, der lokasjonsinformasjon ble gitt i fasekoder og forsinket lateral inhibering mellom overgangscellene. Dette ga høy heksagonalitet i nettverk på 13 og 23 gitterceller. I tillegg presenteres en flerseksjonsmodell av overgangsceller med dendrittiske beregninger for å erstatte stedbaseret lokasjonsinformasjon med grensevektor informasjon. Resultater tyder på at overgangscelledendritter bør respondere til enkeltsteder, men jevnt fordelt i miljøet. Arbeid etterlater også åpne spørsmål om populasjonsaktivitet i overgangscellenettverk. Til slutt presenteres også en modell for produksjon av stedcellesekvenser uten å bruke bakoverpropagering. Totalt utgjør dette verket et argument i favør mulig biologisk implementasjon av TSS-modellen.

# 1 Introduction

## 1.1 Animal Navigation

A striking observation from the technological strides made in modern time is how difficult engineering robots that are able to localize and navigate autonomously is, despite how widespread it is in the animal kingdom. It is tempting to consider the striking feats of pathfinding, like birds trekking thousands of kilometers each year, following the same routes each year, or salmon returning to their home rivers after spending their adult lives in oceans half a world away. However, just looking at rodents' ability to flexibly navigate a variety of different mazes, independently of the maze's structure or the sensory cues available, and react appropriately to novel environments or changes, after only a short time of exploration, has been a mystery for decades (Wynn and Liedvogel 2023).

Studying rodent navigation in a laboratory setting initially belonged to the field of psychology, before the study of the neuron, neuroscience, was properly established. Without methods for investigating the living rodent brain, numerous studies were still conducted to determine their navigational capabilities. In the 1940s, psychologist Edward Tolman conducted numerous such experiments, leading him to a conclusion that has had ramifications for the study of the brain since.

In 1946, for instance, he set up the sunburst maze to test rodent pathfinding (Tolman, Ritchie, and Kalish 1946): rats would enter a circular room from a southern arm, and the only other exit from this room was a corridor leaving from the north. Following this exit, the rodents were taken through a twisting corridor which eventually led to a food reward, in a position that was north-east of the initial room. After doing this multiple times, learning that a food reward existed at the end of the northern corridor, the rats would enter the same hub, but with the northern arm blocked. Now, multiple other corridors had been added to the room, going in different varying directions from west, north west, north east and east. Although rats had only explored the northern pathway previously, with it blocked they preferred a corridor taking them towards the north-east.

By the looks of it, the rats were aware of the geographic direction from the circular room to the food - the conditional learning they had undergone was something more than just learning that going forward and going through the winding corridor would lead to food. In a subsequent 1948-paper, Tolman described his conclusion - the rats have a cognitive map, an internal representation of the environment that would allow them to react flexibly to changes in the environment (Tolman 1948). The more accurate this internal representation is, he argued, the better the rats would be able to navigate.

Parallel to the development of neuroscience in the following decades, shedding light on the way cognitive maps could occur in brains, the rodent's ability to navigate has been studied further. A central goal was to determine what type of sensory information rodents rely on: particularly, do they navigate well with only self-motion cues, such as vestibular or proprioceptive inputs, or do they rely on information about the external world too (Dudchenko 2010)?

Using primarily self-motion cues, path integration allows deducing current position relative to a goal based on past movements by keeping track of travelled distance and direction. This method of navigation would be highly useful: it does not rely on the presence of any external information, so it

reflects the flexibility seen in animal navigation. However, if the path integration system is prone to noise or bias, it quickly accumulates error (Cheung et al. 2007). In an interesting study, a research group tested this in hamsters by removing them from their nest, and tracking their movement in pitch darkness (Etienne et al. 1986). The nests would typically be located at the edge of a circular environment, and the hamsters would be placed in the center. Hamsters showed an ability to home directly towards their nest. However, if the environment was subtly rotated while the hamster was being moved, some hamsters would try to move in the direction their nest would have been in, if no rotation occurred. Others found the path to the nest right away. This indicates that at least some hamsters guessed the location of their nest without using external cues. Multiple other studies have shown that rodents can navigate and home effectively without getting external information, but experiments are also clear that this only works in a limited capacity, for humans and rodents alike (Kim et al. 2013). If the path is too long or involves too many turns, landmarks or external information is probably necessary for accurate navigation.

However, other studies have shown that rodents also rely on visual landmarks (Dudchenko 2010). One example is a study from a radial arm maze, in which eight or more arms all meet in a central intersection. At the dead end of each arm are food rewards, and on walls outside the maze are visual cues, serving as landmarks. Normally, when subjected to such a maze, a rodent will visit each arm on average once, retrieving the food and then not returning to that arm again by accident, requiring some memory of where it has already been (Suzuki, Augerinos, and Black 1980). However, if the landmarks are shuffled or rotated after three food-items have been retrieved, the same accuracy is not maintained.

Studies on animal navigation are numerous, and a series of other mazes have been popularized to test navigation. The field is rich, and the observations will not be reproduced in detail here. Rodents are able to integrate multitude of senses during navigation, both path integration and external landmarks, to tell where they are in an internal, cognitive map of the environment. They are also able to tell their position relative to their goals, and plan paths depending on blockades and new information.

## 1.2 The Transition Scale-Space Model

The Transition Scale-Space (TSS) model was developed and published only a few years ago (Waniek 2020). It extends Tolman's notion of a cognitive map, and can be abstracted beyond spatial maps. However, it is readily adapted to a spatial context. At its base is the following observation: to properly navigate, an animal would benefit from two distinct cognitive maps, instead of one. One map of the world, a type of memory which represents all experienced locations, and one map of transitions, how to get from one location to a neighbor.

In this context, the place-map only needs to contain information about isolated positions, without regard to how they are connected. The TSS model also works with the neuron as the base unit, and based on experimental evidence, the fundamental unit of the place-map is a place cell, which encodes some location in an environment. These place cells can be activated from external landmark information alone, the TSS-model posits, and a place cell can give information about the nature of

the place - did the rodent previously encourage a predator when that place cell was active, or is the place cell in the middle of its nest?

However, the TSS-model places emphasis on the second network, the transition network, which can accelerate the retrieval of place cell sequences between goal- and target places. The unit of this network is the transition cell, which remembers some set of possible spatial transitions. The transition cell could be observed in multiple ways, but there are a few ways to optimize it: for one, a transition cell should represent as many spatial transitions as possible, and secondly, it should retrieve place cell sequences as quickly as possible, so the animal needs to spend as little time as possible evaluating the best path.

From the perspective of the TSS-model, if the rodent brain has evolved a transition network, it would be optimized. Using graph theory and propositional logic (see Waniek 2018), the TSS model reasons in the following way about this transition network: while a transition neuron should encode as many transitions as possible, it must not encode transitions to and from the same place. Consider places A, B and C that are all consecutive on a linear track, and represented by each their place cell, cell a, b and c. To get from place A to C, one must pass through place B. If a single transition cell encodes both transitions from place cell a to b as well as b to c, it may produce the unwanted place cell sequence  $a \rightarrow c$ , while the wanted sequence is  $a \rightarrow b \rightarrow c$ .

Under this constraint, the TSS model proposes a transition cell with the following activity pattern: for one, it will represent transitions from some circular region in space, called a center-area, and transitions to an annulus surrounding this circle, called a surround-area (figure 1.1). As such, any transition from a place cell with receptive field within the center-area to a place-cell with a receptive field within the surround-area is considered a valid transition by this transition cell.

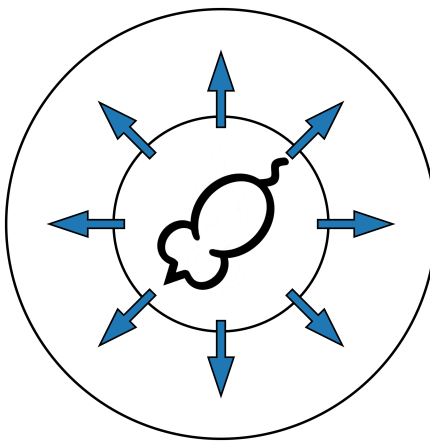


Figure 1.1: Illustration of single center/surround region of transition cell. The transition cell should encode all spatial transitions from within the central circle (center area) to the surrounding annulus (surround area) as indicated by arrows. Adapted from Waniek 2023.

On top of this, the transition cell will try to bundle as many of these center-surround-complexes into an environment as possible, as long as the surround-area of one complex is not overlapping the center-area of another.

The transition cell would be active in any of the center areas, to give information about which places exist in the surrounding area. With this activity pattern, and optimally placed center-surround complexes, the transition cell would be active in a hexagonal pattern across the environment (Waniek 2018; Kunsch, Agrell, and Hamprecht 2005). Due to its periodicity, only three transition cells are necessary to make sure that all places in all environments are covered by a transition cell's center-area.

In any given position, a place cell will be active, giving information about current position, and some number of transition cells will be active, giving information about places in the surround area.

In further work, Waniek determined that transition cells should operate under different scales, in which each scale represents the size of the center-surround regions (Waniek 2020). This would

accelerate the rate of producing place-sequences, which was another optimization for the transition network. To accelerate sequence-retrieval, having multiple scales with increments of  $\sqrt{2}$  from one scale to the next was shown to be optimal. An estimated 7 - 9 scales would cover all behaviorally relevant scales.

As mentioned, this model can be seen as a conceptual extension to Tolman's cognitive map: a single map isn't ideal, because both the localization information and the relational information should be stored. As will be shown in the upcoming section, the TSS model was also based on a large experimental body of observations of the rodent brain that has been found since Tolman. With this basis, the TSS-model shows that by splitting the localization- and relation-networks in two, the relational memory can both optimally accelerate finding sequences in the place-network while consisting of a finite number of highly efficient transition cells.

## 1.3 Spatial Cell Types in the Hippocampal Area

### 1.3.1 Place cells

Around the same time Tolman published his thoughts the cognitive ma, the cellular unit of the brain was characterized - the spiking neuron (Hodgkin and Huxley 1952). Neurons receive inputs from other neurons in rich dendritic trees, and these inputs are converted to membrane voltage potentials in the neuron. If the voltage exceeds a threshold, the neuron's axon depolarizes in an all-or-nothing action potential, making the neuron release an output of its own. These outputs are typically transmitted to other neurons over synapses.

This formed the foundation of neurons as we understand them today. In 1971 a link between the neuron and Tolman's cognitive map was established in the place cell (O'Keefe and Dostrovsky 1976; O'Keefe 1976). This cell was found in the hippocampus, a part of the brain initially studied due to its relevance in episodic memory. The place cell had one striking feature - while the mouse studied ran around in a square box, the cell would only be active if the mouse was within some region of the box. The place cell had a single preferred location in the box, and the closer the animal was to that place, the higher its firing frequency would be. Located in a part of the brain associated with memory and memory formation, it was a good candidate for a unit in a cognitive map. It has been the object of intense study since, leading to numerous important observations.

The hippocampus is subdivided into multiple regions, of which three have received most attention: the dentate gyrus, the CA3 and CA1 (Cherubini and Miles 2015). The dentate gyrus receives inputs from outside the hippocampus, downstream of numerous sensory modalities. The CA3-region receives inputs from the dentate gyrus, is recurrently connected, and projects to CA1. CA1 gives outputs to the subiculum, which is outside the hippocampus proper and communicates with the prefrontal cortex. The pathway from dentate gyrus as an input structure, via CA1 and CA3 to the subiculum, is called the trisynaptic circuit. For long, this circuit was thought principal for hippocampal activity, but evidence suggests that CA1 also receives direct inputs from parahippocampal areas (Kerr et al. 2007). Place cells have been found in both CA3 and CA1, showing similar properties (Dong, Madar, and Sheffield 2021). Curiously, place cells have not been found in other brain

areas, and additionally, severing the connection from CA3 to CA1 does not diminish CA1 place cell activity significantly (Brun et al. 2002).

Within CA3 and CA1, only a fraction of the cells will behave as place cells in some environment. However, as a population, these cells can cover the environment, making the foundation of a spatial cognitive map (Wilson and McNaughton 1993). Moreover, upon changing environments, the networks undergo orthogonal, global remapping - some place cells will remain as place cells, others will not, and there is no correlation between the places they occupy in one environment and another (Muller and Kubie 1987). If the environment is changed, such as changing the color on the walls or an underlying olfactory cue, some place cells remap, others do not - partial remapping (Anderson and Jeffrey 2013). This implies that place cell activity is somehow context dependent, although the cause and purpose of this is unknown.

The hippocampus and surrounding regions exhibit oscillatory local field potentials during locomotion (Wilson 1978). The periodicity is typically between 4 and 11 Hz, and place cell activity has been found to depend on the phase of this wave (O'Keefe and Reese 1993; Skaggs et al. 1996; Hafting et al. 2008). During locomotion, the place cell that is most active in the current position will activate at the trough of the theta phase, a place cell whose most active position was recently passed will activate a little earlier, and a place cell whose most active position will shortly arrive will activate a little later, in the descending or ascending parts of the theta cycle, correspondingly.

This phenomenon, called theta phase precession, shows that the phase-timing of the place cell gives some information about the time the animal will reach that place, but it also leads to preplay (Dragoi and Tonegawa 2011; Dragoi and Tonegawa 2013). The way place cells activate related to phase means that each theta-cycle, a short sequence of place cells will activate consecutively, starting with place cells representing places the animals just were, and ending with place cells its shortly going to arrive at. Curiously, this also applied when the animal explored a novel environment, activating place cells it had never been at.

A separate phenomenon was discovered before preplay, called replay, and occurs during sleep or rest after navigation (Wilson and McNaughton 1994; Olafsdottir, Carpenter, and Barry 2016). In the study that first discovered this, the animal ran along a track, so the same sequence of place cells activated repeatedly. Following this, during sleep, the same sequence was replayed, forwards and backwards, but compressed significantly in time. Curiously, reverse replay is seen more frequently after increasing reward (Ambrosa, Pfeiffer, and Foster 2013).

The networks of hippocampal place cells is a candidate for a cognitive map of the rodent's spatial environment, as described by Tolman. The remapping, theta phase precession and replay are some of its distinguishing features, implying that the network both has some concept of context and of spatial sequences. However, it is not clear what neural inputs the place cell uses to compute place fields, what causes remapping or how preplay and replay is generated. One brain area of interest in this context was the hippocampus' main input structure - the entorhinal cortex. In this region, multiple spatially modulated neurons have since been found, the most striking of which might be the grid cell.

### 1.3.2 Grid Cells

The entorhinal cortex was investigated because it was one synapse upstream of the hippocampus. In 2004, this lead to the discovery of the grid cell, characterized by a periodic, hexagonal spatial firing field that spanned the environment (Hafting et al. 2005). Grid cells were first found in the second layer of the medial entorhinal cortex (mECII) but have since been found in the third and fifth layer (mECIII and mECV), as well as in the pre- and para-subiculum (Boccara et al. 2010). In the mECII, hexagonal activity has been observed in both stellate and pyramidal principal cells (Rowland et al. 2018). As such, this hexagonal firing pattern is widespread in the parahippocampal area, but its purpose is still undetermined.

The hexagonal acivity pattern of grid cells is characterized by three primary variables - the scale of the grid, its orientation relative to the environment and its phase. Grid cells in mECII that are physically close tend to have similar scale, orientation and phase (Hafting et al. 2005). In square environments, grid cells typically coalign with a 7.5 degree orientation offset relative to one environment wall (Stensola et al. 2015). Meanwhile, grid cell scale increases discretely and geometrically in grid cells along the dorsoventral axis of the mEC, increasing by a factor between 1.4 and 1.7 from one scale to the next (Stensola et al. 2012). This indicates that grid cells belong to modules, in which all cells within a module share orientation and scale, but scale varies between modules. Within a module, grid cells have varying degrees of firing field overlap, depending on their relative phases.

On a whole, grid cells firing fields are noted for their robustness - in rats, their firing field is maintained in the absence of sensory inputs, indicating a measure of path integration, and firing in pure grid cells is independent on animal velocity and heading direction (Hafting et al. 2005). While they show theta phase precession similar to hippocampal place cells, they do not remap orthogonally, as grid cells maintain their relative orientation, phase and scale compared to other grid cells in the network when environments change (Hafting et al. 2008; Fyhn et al. 2007). However, grid cells do not always show hexagonal patterns, for instance seeing sheared fields in sufficiently large environments or in environments of non-regular shape (Stensola et al. 2015; Krupic et al. 2015).

Topological analysis has captured these features in the population activity across a grid cell module (Gardner et al. 2022). In narrow time windows, the grid cell population firing can be placed on the manifold of a twisted torus. This indicates that across environments, and regardless of environmental shape or shearing effects, the network is somehow organized so the correlation between two grid cells spiking is maintained, and organizes onto a two-dimensional toroidal surface for the entire module.

The mECII receives inputs from large regions of the brain, but the most notable are neighboring regions CA1, the pre- and parasubiculum, the retrosplenial cortex as well as the post- and perirhinal cortices (Kerr et al. 2007). Lesioning inputs from CA1 has been seen to impair grid cell activity, showing important connectivity from CA1 (Bonnevie et al. 2013). However, as CA1 is downstream of the entorhinal cortex, both directly from mECIII and indirectly via the trisynaptic pathway from mECII, this might not be a satisfactory input structure providing grid cells with spatial information (Tamamaki and Nojyo 1993; Kerr et al. 2007; Witter et al. 2017).

It is not clear how the other main input structures impact grid cells, but in rodents, removing the theta oscillations by disabling the medial septum impaired the hexagonal field (Brandon et al. 2011; Koenig et al. 2011). Curiously, grid cells maintained normal firing without theta oscillations in bats (Yartsev, Witter, and Ulanovsky 2011). More than this, the post- and perirhinal cortices are known to integrate numerous sensory modalities, and multiple spatially modulated neuronal types have been observed in the pre- and parasubiculum, so these can provide spatially modulated sensory inputs to grid cells (Furtak et al. 2007; Groenand and Wyss 1990). Although Hafting et al. 2005 found stable gridness in darkness in rats, Chen et al. 2016 tested gridness in darkness in mice, and found this to be disrupted leading to the conclusion that visual stimulus indeed is important for maintaining grid fields.

In terms of output, mECII grid cells have not been observed to be excitatory recurrently connected. However, multiple studies have confirmed a fast-acting lateral inhibition within mECII by parvalbumin-positive interneurons (Couey et al. 2013; Buetfering, Allen, and Monyer 2014). Maturation of this interneuron layer during development strengthens the grid pattern (Christensen et al. 2021), indicating that these lateral connections are important for the grid field.

The purpose of grid cells is widely discussed, but a few candidates have been suggested. Because the mEC gives inputs to the hippocampus, it was speculated if multiple grid cell modules together could produce place cell activity. However, place cell dependence on grid cells was disproved when grid cells were shown to develop later in development than place cells (postnatal day 16-17 vs 19-20) (Langston et al. 2010; Wills et al. 2010; Wills, Barry, and Cacucci 2012).

Because grid cell firing is maintained in darkness, a suggested function has been path integration, which would indicate that grid cell activity would mostly be predicated on velocity information. Other models, such as the TSS, suggest that grid cells participate in navigation by integrating external sensory information. The striking, hexagonal firing fields, as well as the unclear purpose, has lead to a series of different computational models that focus on different grid cell properties, that will be reviewed in section 1.4.

### 1.3.3 Other Spatially Modulated Cells

Grid- and place cells both have striking firing fields, but they are by no means the only cells that have been found showing some spatial preference. This section will briefly mention some of the others, focusing on their activity pattern and location in the brain.

All the following cell types have been found in the parahippocampal area, including the entorhinal cortex, subiculum and pre/parasubiculum, but not the hippocampus, and are functionally defined (Brandon, Koenig, and Leutgeb 2014). The first of these, the head direction (HD) cell, was first found in 1990 in the parasubiculum, and was since also found in the presubiculum and mEC layer III and V, but, interestingly, not in layer II (Taube, Muller, and James B. Ranck 1990). The HD cell is active independently on the animal's position in an environment, but fires preferentially when the head is turned a given direction - collectively, a population of HD cells can encode all head directions. Pathways giving rise to HD cells have been established, showing that vestibular input is critical for their activity, aided by proprioception and external senses (Taube 2007). Conjunctive

cells have been found in the same brain areas, firing preferentially if the animal is simultaneously on a hexagonal grid and facing a given direction (Sargolini et al. 2006). These conjunctive cells have also not been found in mECII.

Combined with the head direction cells, finding the speed cell showed that there is velocity information present in the entorhinal cortex, as necessary for path-integration (Kropff et al. 2015). These speed cells were found across all layers of the mEC, and the spiking of a cell correlated highly with the animal's future speed 50 - 80 ms in the future.

Boundary vector cells and border cells have been found across all layers of the mEC, as well as in the pre- and parasubiculum and the subiculum (Solstad et al. 2008; Boccaro et al. 2010; Lever et al. 2009). These cells are preferentially active when an environment boundary or border is in some preferred direction - border cells when the boundary is immediately next to the animal, boundary vector cells if the boundary is at some fixed, preferred distance. Recent findings suggest that boundary vector cells in the subiculum alter activity based on environment geometry, aligning with cardinal directions in square environments but not in circular (Muessig et al. 2024). Another type of vector-based spatially modulated cell is the object vector cell, which activates if some environment landmark is both in some preferred direction and distance (Arne Høydal et al. 2019).

Modelling work has shown that boundary vector cells can get their receptive fields to high precision using optic flow (Raudies and Hasselmo 2012). The similarity between the models for head direction cells and this one is that they don't depend on prior knowledge of the environment to explain the cellular activity. This makes them viable candidates as providing spatially modulated information to other cells, such as grid cells or place cells, during exploration.

## 1.4 Existing Grid Cell Models

A multitude of models and model families already exist to explain the wealth of experimental data on grid cells, with differences in their suggested mechanisms for the grid pattern, as well as the purpose of the grid cell. Due to their persistent spiking in darkness, many models assume that grid cells path integrate, accumulating self-movement information to predict current location in the absence of external input. Oscillatory interference (OI) - models seek to explain the theta phase precession in grid cells, and have shown that grid-like activity can be achieved by the interference of multiple oscillators in a cell's membrane potential (Burgess, Barry, and O'Keefe 2007; Zilli and Hasselmo 2010). The OI-model can account for many activity patterns besides the hexagonal grid, but if the different oscillators differ in frequency by a sufficiently small margin, and adapt this based on velocity-inputs, the cell can have a grid-cell-like activity with spacings as observed in experiments. Since the theta oscillations typically is one of the interfering oscillations in OI-models, these models reproduce observations of both theta phase precession and the impaired grid cell firing when theta oscillations are disrupted.

Another set of models suggest grid cells as part of a continuous attractor network (CAN), which can explain persistent grid cell activity during rest or sleep (Yoon et al. 2013; Widloski and Fiete 2014). These models have been implemented with lateral inhibition between grid cells, as observed in mECII (Couey et al. 2013), as long as the strength of the inhibition is inversely proportional

to the overlap of firing fields, so the most active grid cell silences all other grid cells. When the animal moves, this activity is shifted to a grid cell with a neighboring phase. This CAN-model has been supported by the topological analysis of mECII-activity by Gardner et al. 2022, and gained traction in recent years (Sorcher et al. 2023). It has been demonstrated that any such system of path integration still needs regular external input to avoid drift (Cheung et al. 2007; Mulas, Waniek, and Conradt 2016), and the exact inhibitory structure predicted by CAN - networks has not been observed (Zilli 2012).

A third group of models predict that grid-patterns can be learnt by Hebbian learning, in which grid cells get their firing fields by associating to suitable spatial inputs and dissociating from other spatial inputs (Soldatkina, Schonsberg, and Treves 2021). As opposed to the OI- and CAN-models, the driving mechanism of grid cell activity in these feed-forward models is not necessarily self-motion inputs, but that doesn't exclude the possibility that grid cells play a role in path integration. An early idea was to model grid cells with firing fatigue and place cell-like input activity, which was not necessarily hippocampal place cells (Kropff and Treves 2008). In this model, there were two primary factors for learning - competitive firing rates between grid cells, so the total population firing rates were normalized, as well as a firing fatigue, so the current firing rate would be negatively influenced by prolonged high past rates. Grid cells would then associate to place cell inputs based on their mutual firing, and the fatigue prevented the same grid cell from associating to all inputs. While this produced grid like cells, carefully tuned excitatory collaterals between gridcells were necessary to make them share orientation. Later, this excitatory collateral was replaced by inputs from a layer of collateral cells that received both place cell-input and head direction-cell input, so the model produced grid cells with shared orientation in a purely self-organized manner (Si and Treves 2013).

Some models generate grid cells with a center-surround learning rule from place-cell inputs. In these models, grid cells typically associate to place cell inputs with firing fields within a center-area, and dissociate from place cells with firing fields in an annulus around this area. Monsalve-Mercado and Leibold 2020 showed that this learning rule, combined with lateral inhibition, reduced boundary-effects on grid formation and gave a high level of gridness. While the grid cells preferred an orientation around 7.5 degrees relative to the walls in a rectangular environment, in line with experimental results, all grid cells were found in one of three distinct phases. Another feedforward model added a second annulus around the center-surround area, and place cells within this narrow ring were tagged so that new firing fields could only be placed on this (Castro and Aguiar 2014). Moreover, if a place cell would get tagged from two separate firing fields of one grid cell, the weights would potentiate. While this was robust to noise, it is unclear if orientations and phases would align between grid cell.

## 1.5 Grid Cells as Potential Transition Neurons

In line with the current models, TSS proposes place cells as units in a cognitive map of the environment (Waniek 2018). The place cell learns to activate based on spatially modulated sensory inputs, in which each place cell associates to spatial inputs from one area, and lateral inhibition prevents other place cells from activating. This has been explored in models, for instance using boundary

vector cells as inputs (Barry et al. 2006).

The grid cells are suggested as TSS transition cells, collectively forming a transition network. As predicted for transition cells, grid cells typically have a hexagonal activity, and are divided in modules based on their scale, incrementing by a factor close to the  $\sqrt{2}$ , optimal to accelerate sequence retrieval.

To learn these firing fields, TSS posits that transition cells correlate and decorrelate to the same spatial inputs as place cells. As opposed to place cells, transition cells associate to spatial inputs responding to center-regions, and dissociate from inputs in the surrounding-regions, while trying to fit as many center-regions into the environment as possible. This resembles some of the feed-forward models presented above. Similarly to CAN-models, however, TSS suggests that transition cells are interconnected by strong lateral inhibition, to discourage overlapping center-regions.

The connectivity between the place cell network and the transition cell network that enables flexible path-planning is then learnt on top of this, based on correlated place- and transition cell activity.

A learning rule for transition cells has been shown to produce grid cell-like transition cells in discrete-time simulations. In these simulations, transition cell networks consisted of three transition cells, the smallest possible number to cover the entire environment, and the transition cells received place-like inputs sampled from a regular, rectangular grid of spatial afferents (Waniek 2017). In discrete time-steps, activity in the spatial cell layer would activate transition cells depending on a position in a simulated trajectory. Following this, three separate learning rules would update input-to-transition cell weights. The first rule would let the most active transition cell associate to the central spatial cells, and dissociate from surrounding spatial cells. The second rule, called the baseline, would increase the weights from the active input cells to all transition cells, for both active and inactive transition cells. Third, an interaction rule would weaken the connection from inputs to all transition cells except the most active one. A rationale for the three learning rules is that the first rule provides the center-surround effect necessary for transitions, the baseline encourages transition cells to be active as frequently as possible to encourage effective transition cells, and the interaction rule discourages excessive overlap between transition areas.

Although this network gave cells with high gridness in networks of three transition cells, it was not explored in bigger networks. Additionally, it is unlikely that a biological network providing the spatial inputs shows regularly distributed, place like activity, at least prior to exploring the environment. Both of these constraints need to be addressed for the TSS model to be considered biologically plausible.

## 1.6 Thesis Goal

A general objective of this work is to investigate biologically implausible aspects of the TSS-model as it currently stands. Primarily, this relates to the spatial learning of transition cells, with two primary aims: 1) establish the transition cell network described in the section above in a more biologically plausible way to see if cells develop gridness in networks of more than 3 transition cells, and 2) explore the role of spatial input on transition cell activiy. Next to these, appendix A

presents a model for computing place-cell sequences under the TSS, using continuous time and spike delay-learning, as opposed to backpropagation used in past simulations (Waniek 2018).

The first of the two primary aims is investigated by simulating a transition cell network in continuous time with delayed inhibition. The hypothesis is that this delayed inhibition allows multiple transition cells to develop gridness by partly overlapping their firing fields. The network should resemble the previous simulation as much as possible, to allow some level of comparison.

Second, the way the structure of spatial input affects gridness is also explored. This is both to see if using rectangularly spaced inputs is necessary to produce gridness, and to evaluate the possibility of vector-based inputs such as BVCs, instead of place-like inputs.

With a simple STDP- based learning rule, along with a baseline weight modulation, transition cells developed high gridness levels in larger networks than previously observed, and in with multiple network structures. This is an argument that cells can learn spatial transitions effectively under biologically plausible conditions. However, gridness did not occur in models with BVC-inputs, and it is unclear if this is because of the overall model design or the choice of hyperparameters.

## 2 Methods

### 2.1 Overall model design

This thesis seeks to test gridness in transition neurons as described by the TSS-model with biologically plausible conditions. To achieve this, transition cells were simulated in a spiking neural network, which are artificial neural networks with certain properties:

1. The network is simulated in continuous time, or with time steps that are vastly shorter than the mean firing rate of neurons.
2. Neurons communicate in temporally discrete spikes, triggered when an internal voltage variable exceeds a threshold.

In addition to these properties, an ideal network must meet more requirements to be considered biologically plausible in this work. First, all communication should happen at a temporal delay. Second, learning rules must be online and local. Online and local learning rules mean that all variables necessary for learning must be available at the time of learning (online) and in the physical location where learning occurs, typically the synapse (local) (Veen 2022).

Spike timing dependent plasticity (STDP) is a learning rule in which a synapse updates weights both when the presynaptic and the postsynaptic neuron spikes (Song, Miller, and Abbott 2000). The weight-update is according to a STDP-kernel, in which weights are decreased upon presynaptic activity and increased on postsynaptic activity. The magnitude of weight decrease is high if there was a postsynaptic spike shortly before the presynaptic inputs, and the magnitude of weight increase is high if there was a presynaptic spike shortly before postsynaptic activity. The processes of decreasing and increasing weights do not need to be symmetric. By the conditions above, STDP is a biologically plausible learning rule.

A baseline learning rule increments weights slightly when a presynaptic neuron is active, regardless of postsynaptic activity. This learning rule is also online and local, satisfying all constraints.

Next, an ideal network should get inputs from some plausible spatially tuned neuron type, more precisely boundary vector cells (BVCs), whose activity is based on real or simulated trajectory data (Lever et al. 2009). From these inputs, another layer of cells of arbitrary size learns center- and surrounding area information to represent transition-cells as described in the TSS-model, encoding transitions on a single scale. The reason BVCs are considered plausible is that their activity can be maintained even when exploring novel environments (see Raudies and Hasselmo 2012).

Finally, an ideal network is not dependent on highly specific parameters, and shows some robustness to noise, which is likely necessary for any actual brain network.

Under these constraints for plausibility, the aim of the work is to test whether transition neurons self-organize into modules with hexagonal activity patterns in space, and if this is in line with experimental results of gridcells in the mECII, as predicted by the TSS model (Waniek 2018).

Both an ideal network and subsequent simplifications will have some common features to accommodate these objectives: To facilitate STDP, which allows center-surround learning, all inputs arrive in pulses at theta-wave frequency set at 10 Hz, in which only spatial input with sufficient

relevance is active (figure 2.1 (a)). The input is also phase coded, so the less relevant it is, the higher the temporal offset is relative to theta (figure 2.1 (b)). This means that a transition cell is likely to fire following center-inputs, and following receive a wave of inputs from cells representing surrounding locations. The STDP learning-rule will encourage potentiation of the center-activity, which arrived pre-spike, while the surround-activity arriving post-spike is depressed. Secondarily, all active inputs are slightly potentiated to encourage the transition cell to be active in as many center-areas across the environment as possible, according to a baseline-learning rule (see equations 3 and 4 for implementations).

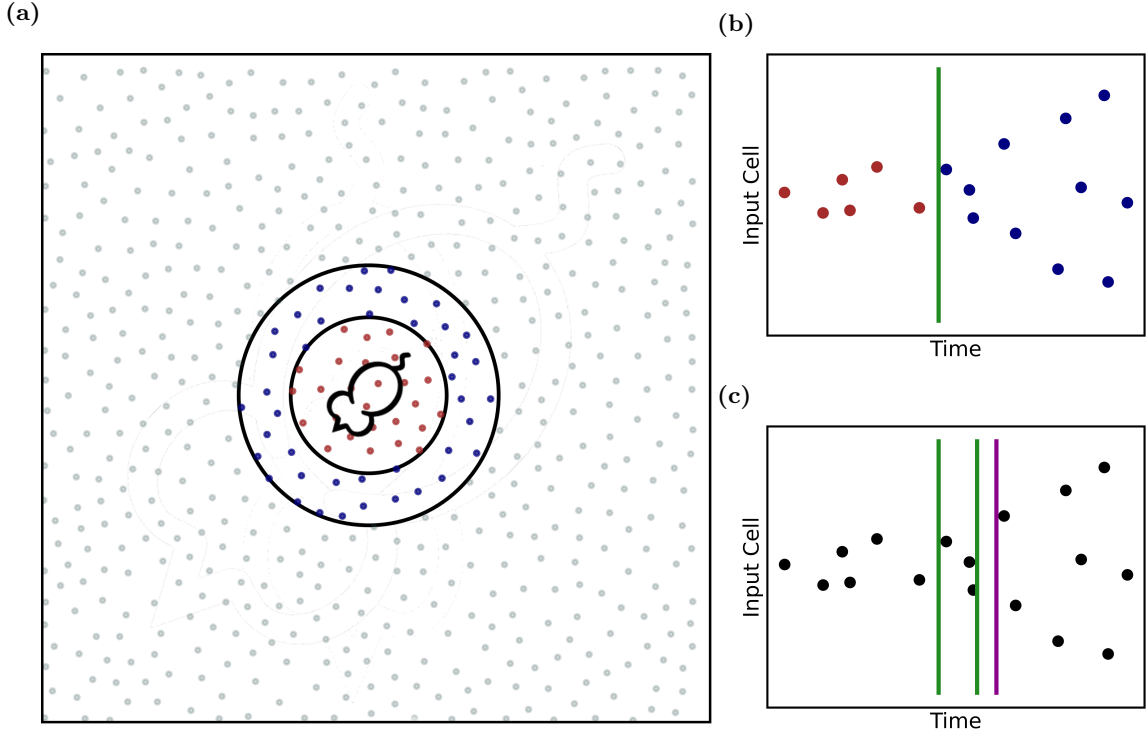


Figure 2.1: The nature of phase coded spatial inputs. (a) Spatial inputs from a region surrounding the mouse will be activated each theta-cycle (10 Hz), here indicated by points within the two surrounding circles. This input is phase-coded, so cells responding to locations closest to the mouse will activate first. (b) Hypothetical raster plot showing input activity in one theta cycle. The spike time of a transition cell (green vertical line) determines which inputs the transition cell will associate to and dissociate from. In this case, the transition cell associates to the inputs colored red (left of the vertical line), and dissociate from the inputs colored blue (right of the vertical line). Comparing to the inputs' locations in (a) (color coding preserved), this can encourage center-surround learning. (c) Delayed inhibition (purple vertical line, rightmost) can allow multiple transition cells (green vertical lines, middle and left) to fire during the same theta-cycle.

An inhibitory layer connects transition cells laterally, causing strong inhibition, but on a delay. This leaves a narrow window in which multiple transition cells can fire, followed by complete inhibition in which no transition cell can fire for the remainder of the theta cycle (figure 2.1 (c)). The window can allow so some transition cells partially associate to the same areas.

## 2.2 Considering BVC inputs

One goal of this work was to obtain grid cell-like transition cells with BVC inputs, and a way to model this is with a direct connection between the two with transition cells as leaky integrate-and-fire (LIF) neurons. In this kind of model, transition cell activity is based on linear summation of BVC

inputs. There are reasons to think that such a network is difficult to achieve. The following idea explains this: in square environments, one could imagine picking two locations that the transition cell has associated to, denoted  $(x_1, y_1)$  and  $(x_2, y_2)$ , and that should make up two firing fields in the hexagonal pattern. In locations  $(x_1, y_1)$  and  $(x_2, y_1)$ , the input would be highly similar to half the input from position 1 and half the input from position 2, due to the nature of BVCs. Notably, though, the transition cell should not fire in these locations, because that would likely lead to rectangular grid firing patterns, not hexagonal. This would be true for all pairs of firing fields that are not parallel to one of the walls. In other words, square environments and linear summation of BVC inputs is expected to encourage rectangular fields, not hexagonal.

It should be noted here that the spiking neural network itself has non-linear features, such as the discrete spiking, that can enable this kind of network to produce grid-cells. One way to achieve this would be with other transition cells that are sufficiently active in location  $(x_1, y_2)$  and  $(x_2, y_1)$ , so they inhibit the first transition cell. However, due to the fine-tuning such a network would require, alternative network structures were preferred.

One such alternative, which highlights an advantage of biological neurons over simplified artificial ones, appears after considering nonlinear dendritic computation in transition cells in a multi-compartment model. This kind of model still implies that boundary vector cells synapse onto transition cells directly, but the simulation treats dendrites as separate units within one transition cell (see figure 2.4 for schematic). Each dendrite would receive inputs from some subset of BVCs, and the transition cell can associate and dissociate to all inputs on an entire dendrite. Similarly to the BVC-model (Barry et al. 2006), each dendrite would preferentially be active in only single locations in the environment. This could be achieved by for instance responding non-linearly to BVC-inputs with a soft-max activation function. In the example above, this would let the transition cell associate to dendrites responding highly to places  $(x_1, y_1)$  or  $(x_2, y_2)$ , while remaining dissociated from dendrites activated in  $(x_1, y_2)$  or  $(x_2, y_1)$ , without sacrificing biological plausibility. This multi-compartment model is in line with the ideal model described in section 2.1.

However, to shorten simulation time and reduce complexity, this kind of network can be simplified. This can be done incrementally, in which each step reduces complexity at the cost of plausibility:

1. The BVC-model showed that place-like activity can be produced from BVC-inputs. As such, BVC-input can be replaced by place-like inputs directly, but still synapsing on non-spiking dendrites in a multi-compartment model.
2. To reduce the number of neurons, each dendrite can connect to each grid-cell, and the dendrites can be spiking to reduce computational time for each of them. Here, the dendrites still fire in random places, according to some distribution.
3. The dendrites can respond to places distributed in a regular, rectangular grid.

Note that step 3 is highly similar to the already existing simulations in (Waniek 2017), just here in a spiking neural network. This was useful, because it allowed testing the hypothesis that transition cells can produce grid-like behavior in networks of more than three neurons if the inhibition

is delayed, not showed in previous simulations. Then, networks could gradually be made more complex and biologically plausible, leading to a series of networks that could be tested sequentially from simple and less plausible to more complex and more plausible. The concrete implementation of each network and other considerations are treated in their own upcoming subsections.

### 2.3 Rectangularly spaced inputs

Consider a model in which transition cells receive inputs that respond preferentially to a single spatial location, and all inputs are distributed on a regular, rectangular grid spanning the entire environment. The importance of this model is twofold: it is closely related to previous TSS-simulations, and is an ideal place to investigate if larger networks still give gridness. Moreover, as outlined in section 2.2, it provides a useful stepping stone to subsequent models.

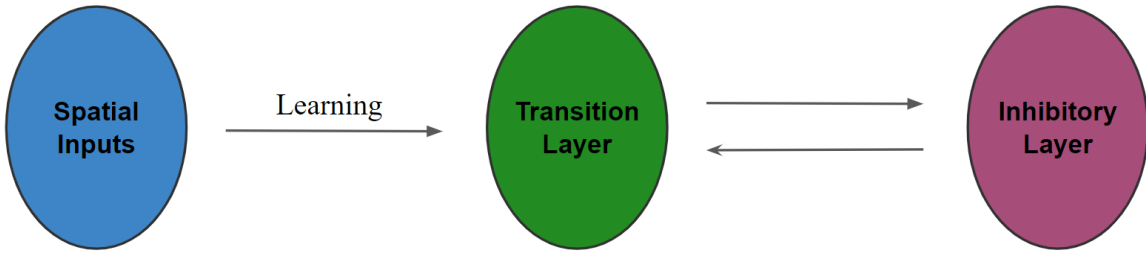


Figure 2.2: A linear summation network structure with lateral inhibition. Each transition cell receives the same spatial input, typically place-modulated cells, and spikes when an internal voltage variable surpasses a threshold. Inhibitory neurons are activated at a delay, and inhibit the entire transition cell network equally. Learning occurs on the input-to-transition cell weights, with a dual STDP-baseline learning rule.

The network has three main layers: input neurons, transition cells and inhibitory neurons (figure 2.2). The input neurons have a preferred spatial location, and have the chance of being activated each theta cycle, which is set to happen with a 10 Hz frequency. The activation function for input neuron  $i$  with position  $(x_i, y_i)$  is given in equation 1.

$$d = \frac{\sqrt{(x_i - x)^2 + (y_i - y)^2}}{\sigma} + \mu \quad (1)$$

Here,  $d$  is the phase-coded spike time relative to theta (in milliseconds),  $x$  and  $y$  is the current location in cartesian coordinates,  $\sigma$  is a scale parameter determining the width of input and  $\mu$  is a noise term. Typically, there was a cutoff at 20 ms, so only reasonably active inputs would activate, but this cutoff was arbitrary, and could for instance depend on the transition cell scale. In this model, inputs would be distributed in a rectangular, even grid across the environment.

Each of these inputs synapses on each transition cell, with weights initialized randomly from a uniform distribution, between 0 and some maximum,  $w_{max}$ . The transition cell was modelled as an LIF-neuron, with a voltage parameter which triggered spikes if it surpassed a threshold, or updated according to equation 2.

$$v(t+1) = \begin{cases} 0 & \text{if } v(t) > \text{threshold or refractory} \\ v(t) - e^{-(v(t))/\tau} + \sum_0^i (w_i \cdot i(t-d)) & \text{otherwise} \end{cases} \quad (2)$$

Here,  $v(t)$  is the voltage of time,  $\tau$  is a decay parameter,  $w_i$  is the weight of the  $i$ th input and  $i(t - delay)$  is 1 if input  $i$  spiked at time  $t - d$ , in which  $d$  is the input delay, and 0 otherwise.

The STDP learning rule was implemented by separating potentiation and depression: upon transition cell firing, potentiation for weight  $i$  would increment dependent on presynaptic activity (equation 3).

$$w_i = \max(w_i + a_i^{pre} \cdot \nu_t, 0) \quad (3)$$

Here,  $a_i^{pre}$  is a variable incremented when input  $i$  fires, and decays with time.  $\nu$  is here a learning rate, which was modulated by animal running speed according to equation 5. Similarly, upon presynaptic input from input  $i$ , weights are depressed if the input arrives after transition cell spike. Regardless of transition cell activity, the input weight would also increase according to a baseline parameter. Both of these rules are captured in equation 4.

$$w_i = \max(w_i + (a_i^{post} + \alpha \cdot (w_{max} - w_i)) \cdot \nu_t, 0) \quad (4)$$

$a_i^{post}$  is a symmetric parameter to  $a_i^{pre}$ , but which decrements upon post synaptic firing and decays at a separate rate.  $\alpha$  determines the magnitude of baseline weight increase.

Equation 5 shows learning rate as a function of movement speed at a given time, relative to the mean speed.

$$\nu_t = e^{-(v_{mean} - v_t)^2 / v_{mean}} \quad (5)$$

$\nu_t$  is the learning rate,  $v_{mean}$  is the mean speed across the simulation and  $v_t$  is the animal speed at a given time.

Transition cells then interacted by activating inhibitory neurons which inhibit all transition cells for a time, working by reducing their voltage by a large, constant amount, but which was small enough so the voltage returns to zero by the next theta by equation 2. This inhibition was global and uniform, so each transition cell inhibited all the others and itself equally. Although this inhibition was thought to work with a delay, some simulations tried running without. In these, the delay was at the simulation software's minimum, 0.2 ms. The number of transition cells in a simulation was arbitrary, but typical values chosen were 13, 23 or 37. Too large networks would require high computational resources, and using primes avoided biases from symmetry.

See table 3.1 for typical parameters of this model.

## 2.4 Randomly spaced inputs

An aim of this work was to investigate the role the input structure plays in developing gridness, beyond a rectangular distribution introduced in section 2.3. The network models that tested this were highly reminiscent of those described in the last section, but used inputs of different spatial distributions.

Two distributions were tested, in addition to the rectangular grid given in section 2.3 (figure 2.3): 1) A blue noise pattern, to ensure a relatively even, although not regular, distribution of spatial firing and 2) A white noise pattern, in which one input neuron would respond to areas independently of other areas.

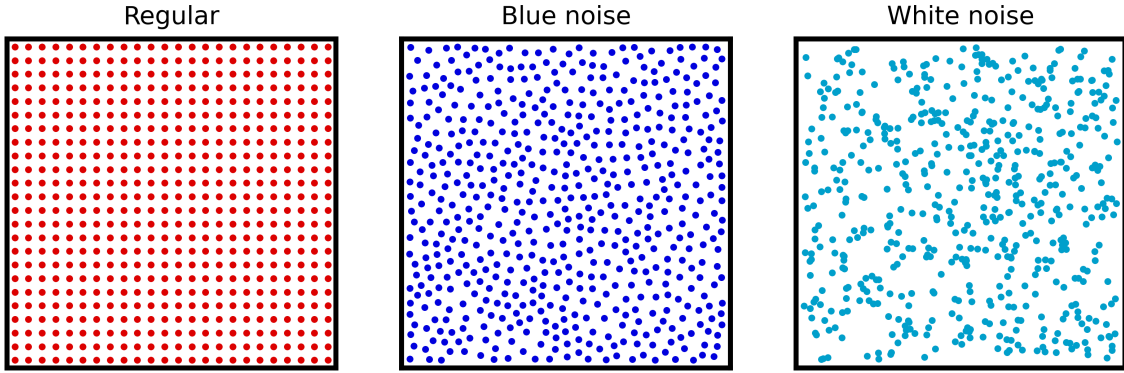


Figure 2.3: Examples of the three kinds of input distributions. Each plot shows 24x24 inputs. Regular distribution places inputs evenly across the entire environment in a rectangular way. A blue noise distribution places inputs sequentially so each is placed as far away from previously placed inputs as possible, resulting in an even, unstructured distribution. White noise distribution places inputs randomly, and independent of all other inputs, so some locations produce more input activity than others.

The blue noise inputs were generated by iteratively suggesting a number of uniformly, independently distributed 2d-points, adding the point that was the furthest from all previously added points to the added points, and repeating until the desired number of added points was reached. To allow for good spread, the number of suggested points was directly proportional to the number of existing points. White noise inputs were generated by getting the desired number of uniformly distributed 2d-points independently of each other.

## 2.5 Multi-Compartment Model

A multi-compartment model was briefly justified in section 2.2, as a way to include non-linear dendritic computations which were interesting for BVC-inputs. The most natural way to implement this in the Brian2, the simulation software used, was as a separate, non-spiking layer between the input-layer and the transition cell layer, and simulate the synapses from dendrites to transition cells as gap junctions (figure 2.4). To test the model with non-spiking dendritic computation without the complexity from BVC-inputs, this multi-compartment model (MC Model) used place-like input cells as an intermediary step between the models in previous sections and a full BVC-input model.

To justify the two-layer neuron model with dendrites and soma as a multi-compartment model, the dendrites had the following properties: they only synapsed onto a single transition cell body, were non-spiking, and the dendrite-to-soma connectivity was modelled as a gap junction, as in (Alabi, Vanderelst, and Minai 2000). In this model, each dendrite only received input from a single input neuron, to simulate the place-oriented dendrite. Each dendrite had a voltage-parameter that would increment by a factor  $w$  when receiving inputs, and decaying to 0 over time (equation 6):

$$v_{den}(t + 1) = v_{den}(t) + e^{-(v_{den}(t))/\tau_{den}} + \sum_0^i (w \cdot i(t - delay)) \quad (6)$$

This resembles equation 2, but does not set voltage to 0 above some threshold, as the dendrite is non-spiking. In terms of inputs, with place-based inputs, each dendrite would only receive input from one input neuron. The weight  $w$  would be a hyperparameter, not changing during a simulation, and was equal for all dendrites.

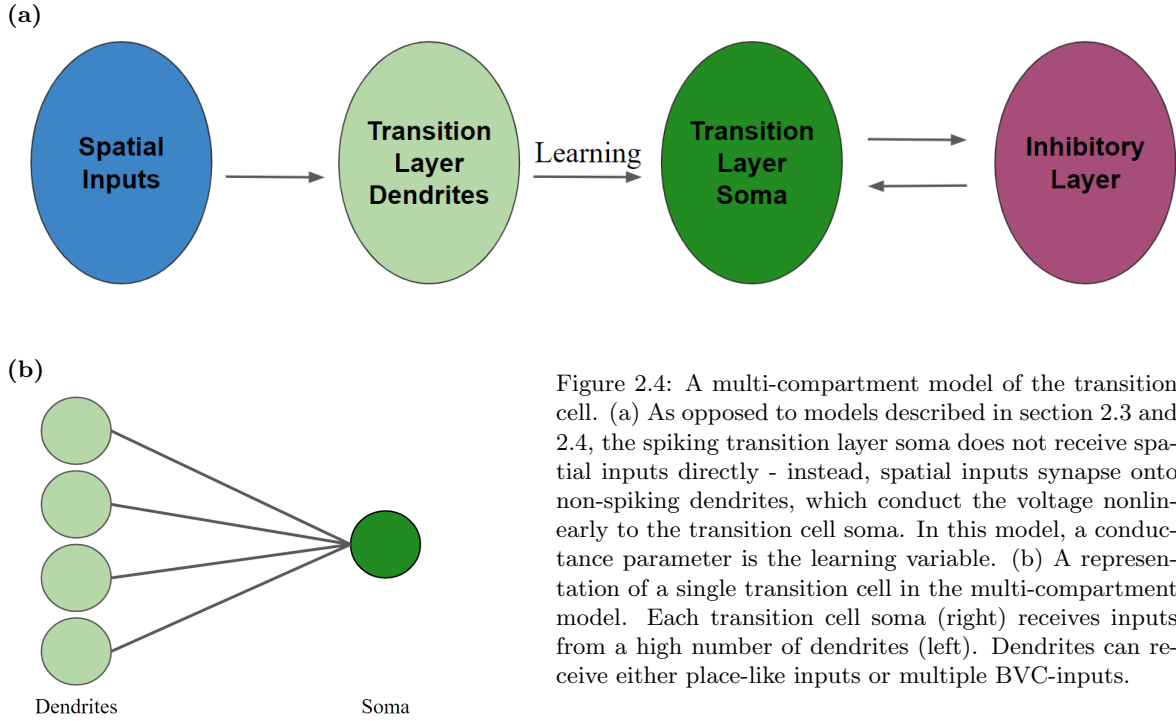


Figure 2.4: A multi-compartment model of the transition cell. (a) As opposed to models described in section 2.3 and 2.4, the spiking transition layer soma does not receive spatial inputs directly - instead, spatial inputs synapse onto non-spiking dendrites, which conduct the voltage nonlinearly to the transition cell soma. In this model, a conductance parameter is the learning variable. (b) A representation of a single transition cell in the multi-compartment model. Each transition cell soma (right) receives inputs from a high number of dendrites (left). Dendrites can receive either place-like inputs or multiple BVC-inputs.

Based on this, the grid cell's voltage was determined by the following equation 7.

$$v_{soma}(t+1) = \begin{cases} 0 & \text{if } v_{soma}(t) > \text{threshold or refractory} \\ z + \sum_i c_i \cdot \tanh(v_i) & \text{otherwise} \end{cases} \quad (7)$$

Here, the nonlinear function  $\tanh(v_i)$  gives the dendrite a softmax-like behavior, so the dendrite at anytime is either activated or not, dependent only on its internal voltage-parameter.  $v_i$  is the voltage of dendrite  $i$ ,  $c_i$  is the corresponding dendrite conductance, reflecting how effectively the dendrite's voltage affects the grid cell voltage. The learning rules from equation 3 and 4 is here learning over conductances ( $v_i$ ) instead of synapse weights, but is otherwise identical.

Inhibitory neurons synapsed on the transition cell soma, and not the dendrites, in line with experimental observations (Buetefring, Allen, and Monyer 2014). As opposed to LIF models, modelling inhibition as an instant reduction in somatic voltage would not work with equation 7, as it would be overwritten next timestep. Instead  $z$  represents an internal inhibition parameter. This parameter is decremented upon receiving inhibitory inputs, and decays to 0 over time (equation 8).

$$y(t+1) = y(t) + e^{-y/\tau_y} + a(t) \quad (8)$$

$\tau_y$  is a decay parameter, typically 20 ms, and  $a(t)$  is some constant value (typically around -2.5 v) if inhibition activated at time  $t$ , 0 otherwise.

With this network structure, simulation times were significantly higher than with direct connection between input cells and transition cells, because the number of dendrites was the product of the number of input cells and the number of transition cells, leading to an increase in parameters. This limited the amount of time spent on this and subsequent models.

## 2.6 Boundary vector cell inputs

The multicompartment model described above was modified so a dendrite received a set of BVCs as inputs instead of place-like cells. The softmax function was tuned so receiving only one or a few BVC-input would not elicit any dendrite activity.

This was begun in a simplified version, in which BVCs responded preferentially to one of the four cardinal directions, north, east, south or west, and with evenly distributed preferred distances. Then, each dendrite received a pair of orthogonal inputs, one from a BVC oriented to the northern or southern wall and one to the eastern or western wall, and the BVCs were carefully paired to give the dendritic tree an evenly spaced, rectangular input field. The activation function for a BVC was simply the distance to the wall in the preferred direction, converted linearly to temporal delay.

While the equation for dendritic voltage was the same (equation 6), the softmax-function for somatic depolarization in equation 7 was replaced with a hard step-function to reduce simulation times (equation 9):

$$v_{soma}(t+1) = \begin{cases} 0, & \text{if } v_{soma}(t) > \text{threshold or refractory} \\ \sum_i c_i \cdot (v_i > v_{threshold}), & \text{otherwise} \end{cases} \quad (9)$$

Compared to equation 7, the dendritic conductance  $c_i$  was multiplied by a boolean which is 1 only for voltages above a threshold,  $v_{threshold}$ . Considering that each dendrite only received two BVC inputs,  $v_{threshold}$  was typically between 1.2 and 1.5 times the fixed BVC-to-dendrite weight, so a dendrite needed both inputs in short succession to pass the step-function threshold.

This also necessitated a change in the STDP-learning rule, since  $a_{pre}$  would increment not when the dendrite received an input, but when it passed the threshold  $v_{threshold}$ .

This model is structured to deliberately convert BVC-inputs to a dendritic tree with activity that resembles the model described in section 2.3: rectangular inputs by carefully pairing orthogonal BVCs on dendrites, and a dendritic model that has replaced a soft-max learning rule with a step-function. Despite these simplifications, made to provide a proof of concept for BVC-inputs, this model did not yield gridlike transition cells like the previous models, halting further exploration.

## 2.7 Other network models

A few other network structures were tried apart from the methods above, but were not explored further because they were considered unsuitable. This section will describe the incentives behind these structures, and how they work.

### 2.7.1 Rate coded inputs

One structure was designed as an alternative to using phase-coded inputs described in section 2.3. The model still relied on dense inputs, so in each position numerous inputs would be active, but their activity was rate-coded. Input cells here were modelled as LIF-neurons, so their voltage would decay to some base-value if the cell was not spiking or receiving inputs. To simulate rate-coded input activity, each input cell's base-voltage was frequently updated depending on animal position.

For relevant spatial inputs, the base-voltage would end up above threshold, leading to spiking. Upon spiking, the voltage was reduced to a value below threshold, and remain there for a short refractory period, before again being affected by the depolarization towards the base-value.

For a rate-code like this, a transition cell provided a feedback-signal to the input layer after spiking, which was tuned to only activating input cells that were close to threshold by that time. Coupled with a STDP learning rule, this network structure allowed transition cells to activate the surround-inputs themselves, which would force a post-pre spike timing, leading to dissociation. A challenge with this model was keeping the input structure stable, because the high firing rate center-inputs frequently would activate shortly after transition cell firing and dissociate. However, with single-cell networks, some measure of center-surround fields was achieved.

This network structure was abandoned because having feedback-connectivity from transition cells to input cells was not in line with the TSS model.

### 2.7.2 Linear Summation BVC model

A simple model using direct BVC-inputs on transition cells modelled transition cells as simple LIF-neurons, integrating BVC-inputs and learning directly on the weights from these. Motivation for why this model was abandoned was given earlier, but this model was tested briefly nonetheless. One way to test the stability of the model was to artificially initiate the network with optimal weights for a hexagonal pattern, and see if it maintained the necessary firing dynamics. This was done by reverse-engineering weights, creating ideal firing patterns for each transition cell, by iterating over a 48 x 48 grid of the environment and increasing weights from inputs relevant to a firing position, decreasing weights from inputs that were irrelevant. This approach was not tried for any other methods, but when it failed to produce clear firing fields in the network, along with the arguments presented in section 2.2, this approach was not pursued further.

### 2.7.3 Linear Multi-compartment Models

Models described in section 2.5 used a multi-compartment model of the neuron to allow dendritic computation to convert vector-based inputs to place-like inputs the transition cell could learn transitions on. In those models, the voltage in a dendrite was transformed to a voltage in the transition cell body through a nonlinear softmax-function. An alternative did not include the softmax transformation, instead modelling the transition cell body voltage as the sum of all dendrite voltages multiplied by conductances (equation 10).

$$v_{soma}(t+1) = \begin{cases} 0, & \text{if } v_{soma}(t) > \text{threshold or refractory} \\ \sum_i c_i \cdot v_i, & \text{otherwise} \end{cases} \quad (10)$$

Variables here have the same interpretation as in equation 7.

This model was not pursued for similar reasons as the model above: with BVC-inputs, a number of dendrites were slightly active with only a single BVC-input, producing similar dynamics (section 2.7.2). Even if the learning rules were thresholded, so the STDP- and baseline-learning rules would

only apply to moderately active dendrites, this errant activity would mean transition cells would activate too much in surround locations, losing circular firing fields.

## 2.8 Simulation software

All models and implementations can be found on github (Insert link here?), and while the simulation data is not available on github due to storage capacity, it is available upon request. All simulations were implemented in python, using the Brian2-library for its flexibility and easy implementation (Stimberg, Brette, and Goodman 2019). With this framework, setting up simulations was straight forward, and allowed time-improvements such as only updating STDP-variables when relevant events occurred, not at every time step. Time steps were typically at 0.1 ms, which was also the minimal synaptic delay.

Simulations with place-inputs used custom simulated trajectories, simulated with 10 ms time steps and a square environment. Position was treated like a continuous variable, with velocity and rotational velocity determined by normal distributions from one time step to the next. In simulations using boundary vectors, the external RatInABox library was used (George et al. 2024).

From the trajectories, spatial inputs were calculated prior to simulations, using either position- or boundary information, and added to a brian2 spikeGeneratorGroup. The network state and weights were stored frequently during simulations.

## 2.9 Analysis

To investigate the firing properties of the network of transition cells, weights were frozen, and the activity of the network was sampled from each position in an even 48 x 48 grid across the environment. In simulations with input noise, each position was sampled 5 times, while they were sampled once without noise (figure 2.5 (a)). This gave data from the network state at one moment, which was subsequently stored as spike trains and then converted to histograms of spatial firing fields. Due to considerable computational time per sample, each simulation was typically sampled only every 5 minutes of simulated time.

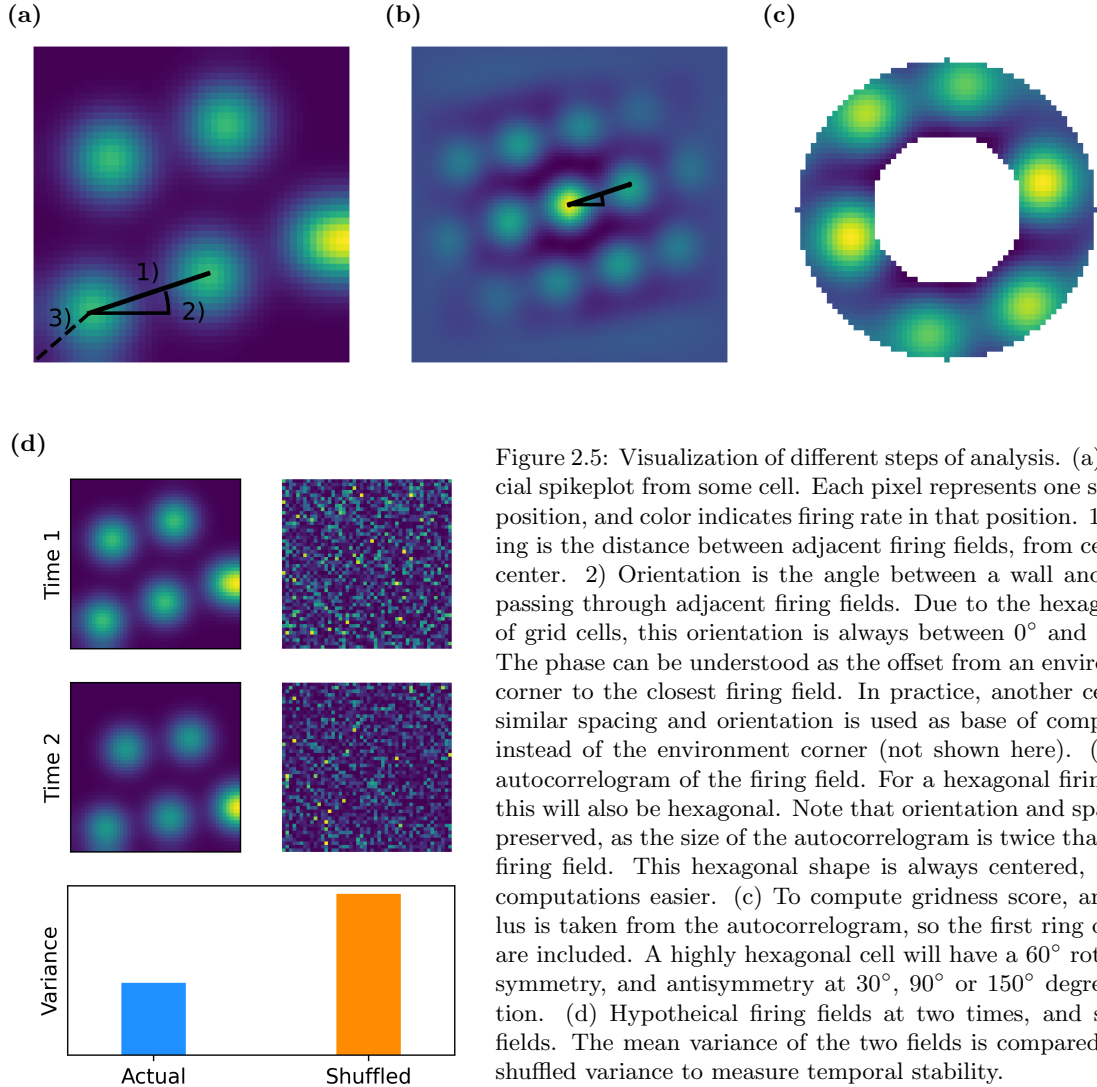


Figure 2.5: Visualization of different steps of analysis. (a) Artificial spikeplot from some cell. Each pixel represents one sampled position, and color indicates firing rate in that position. 1) Spacing is the distance between adjacent firing fields, from center to center. 2) Orientation is the angle between a wall and a line passing through adjacent firing fields. Due to the hexagonality of grid cells, this orientation is always between  $0^\circ$  and  $60^\circ$ . 3) The phase can be understood as the offset from an environment corner to the closest firing field. In practice, another cell with similar spacing and orientation is used as base of comparison, instead of the environment corner (not shown here). (b) The autocorrelogram of the firing field. For a hexagonal firing field, this will also be hexagonal. Note that orientation and spacing is preserved, as the size of the autocorrelogram is twice that of the firing field. This hexagonal shape is always centered, making computations easier. (c) To compute gridness score, an annulus is taken from the autocorrelogram, so the first ring of fields are included. A highly hexagonal cell will have a  $60^\circ$  rotational symmetry, and antisymmetry at  $30^\circ$ ,  $90^\circ$  or  $150^\circ$  degree rotation. (d) Hypothetical firing fields at two times, and shuffled fields. The mean variance of the two fields is compared to the shuffled variance to measure temporal stability.

Five primary variables were derived from each simulation, based on the spatial firing histogram: gridness score, spacing, orientation, phase distribution and temporal stability.

The measure used to evaluate the hexagonality of the transition cells was primarily the gridness score. To find this score, an annulus was extracted around the center of the autocorrelation of the spatial firing fields of a sample (figure 2.5 (a) - (c)). The size of this annulus was estimated to find the first ring of maxima around the center. Using this annulus, gridness score was determined as

$$gscore = \min(a_{60^\circ}, a_{120^\circ}) - \max(a_{30^\circ}, a_{90^\circ}, a_{150^\circ})$$

in which  $a_n^\circ$  is the correlation between the annulus and itself rotated  $n$  degrees around its center.

Gridness spacing was found by evaluating the gridness score with multiple estimations of annulus size, and determining values that gave the highest score (figure 2.5 (a) - (c)). Because of the discretization of space, multiple spacings would give similar scores, in which the middle value was taken.

Orientation was determined only in cells with a positive gridness score. Orientation was determined as the angle between the horizontal line and the first maxima within the annulus, extracted similarly to in the gridness score (figure 2.5 (a) - (c)).

Phase distribution was only evaluated for cells with positive gridness and an orientation between  $-5^\circ$  and  $5^\circ$ , as this was dominant for most simulations (figure 2.5 (a)). In simulations with multiple cells passing these criteria, one cell was chosen at random as a basis for comparison. All other cells would be evaluated relative to this basis by doing a cross correlation, and finding the argument of the maximal value. To find all positions relative to the rhombus, the phase-difference was unsheared, so the rhombus would be rectangular. Then, phase differences could be reduced by a module-operation so all ended up within the same rectangle, and sheared again to be placed within the rhombus.

Temporal stability was estimated by getting the variance in pixel-values in spike plots across time for each cell in the latter half of a simulation, and comparing the mean variances to the mean variance of shuffled pixel values (figure 2.5 (d)). This approach was enabled by the sampling scheme, in which each location in the environment was sampled equally at even time points. Shuffling the spike plots represented the expected temporal stability if there would be no correlation from one timepoint to the next, while a lower variance would imply a positive correlation of firing fields from one time to the next.

Topological structure in population activity was tested in certain networks. Sampled population activity was reduced to the six principal components using PCA, and persistent cohomology was investigated using ripser from the python scikit-tda library (adapted from Gardner et al. 2022).

## 3 Results

### 3.1 Defining Typical Parameters: a Standard Model

Several models were tested in this work. In most of these, overall network structure was kept the same, varying instead on certain parameters that were perceived as critical: the distribution of inputs, inhibition delay, the number of transition cells in a network and the role of noise in the spatial inputs. In addition to these variants, this section will show results from a multi-compartment model with non-spiking dendrites, both with place-like inputs and boundary vector cell inputs. Several hyperparameters could not be explored in detail due to the models' computational demand. In that light, this section will describe typical parameters of one model, and some of the considerations made in setting some of the parameters. This set of typical parameters ends up describing a standard model, which will be used as a baseline for comparison in the rest of the work. This model was chosen as the base model for comparison because it is closest to previous TSS simulations (Waniek 2017).

Table 3.1 shows a typical set of hyperparameters, partially chosen to be biologically plausible, but some sets of parameters were calibrated in order to achieve a wanted dynamic. Since the input was phase-coded relative to theta, weights and spiking threshold were set so the first transition cell would spike typically about halfway between the first input and the phase-delay cutoff. This was thought to encourage even center- surround fields under a STDP learning rule. Inhibitory delay was set to give a brief window for other cells to fire, and is probably shorter than expected biologically (Buetfering, Allen, and Monyer 2014). The apost, apre and baseline was set up to work in conjunction so potentiation and depression would approximately balance each other out, according to equations 3 and 4. The standard model also assumed zero noise in the input phase delay for simplicity.

Table 3.1: Example parameters for simulations. The parameters are partially chosen for biological plausibility, and partly adapted to achieve desired firing dynamics.

Parameter	Value
# Transition cells	13
# Inputs	576 (24x24)
Theta rate	10 Hz
Phase-delay cutoff	20 ms
$\sigma$	0.012
$\mu$	0
Transition cell threshold	1.0
Transition cell $\tau$	10 ms
$w_{max}$	0.14
$w_{init}$	uniform[0-0.75 · $w_{max}$ ]
$A_{pre}$	0.01
$A_{post}$	-0.007
$\tau_{pre}$	8 ms
$\tau_{post}$	80 ms
Baseline	0.005
Inhibitory delay	0.6 ms

The simulations were run on a simulated trajectory, as described in the methods, using a one by one meter square environment. While weights and parameters were stored mid-simulations, data was also extracted from each model by sampling each position in a grid after freezing learning. Figure 3.1 shows sampled cell activity over time in the standard model for seven cells in the same simulation.

Clearly, transition cells typically develop center-surround fields quickly, evidenced already after 5 minutes of exploration from random initial activity patterns.

Five primary variables were quantified about transition cell activity, all using these spike plots. The most central is gridness score, which quantifies the degree to which the firing fields are hexagonal. When finding grid cells in recordings of cell population, a way to qualify cells is by thresholding this score (Sargolini et al. 2006).

The three main variables for looking at grid cell populations were also used for transition cells in these simulations to compare with experimental data: grid spacing, orientation and phase distribution.

Finally, a measure of temporal stability informs about whether the network converges to some state or is shifting. See section 2.9 for computational details.

The following sections will outline results according to these five parameters for ten models:

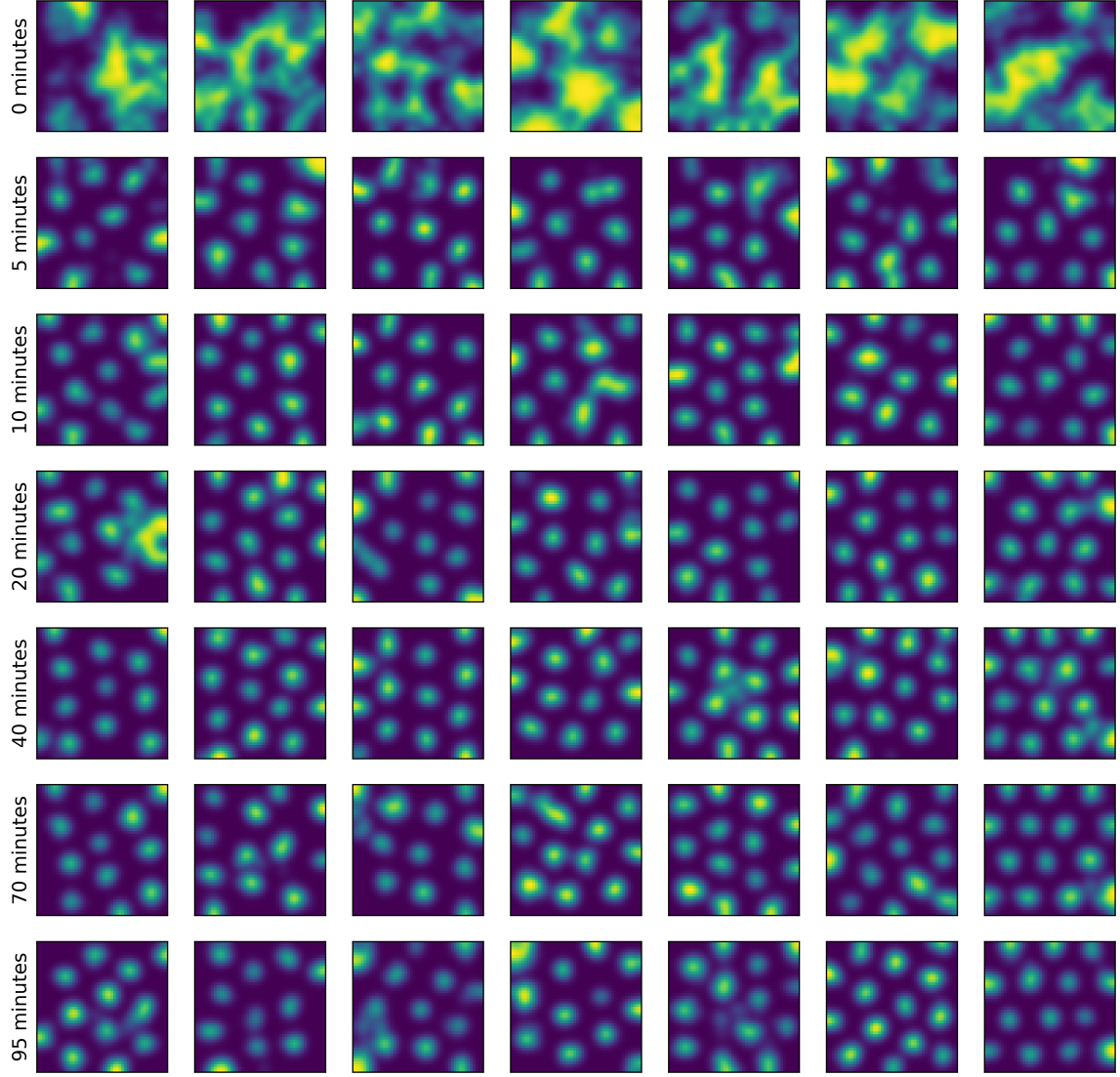


Figure 3.1: Sampled activity from seven transition cells in the same network throughout a simulation. Each plot represents activity in the same  $1 \times 1$  m environment, subdivided into a  $48 \times 48$  grid in which each position was sampled for a single theta cycle. Learning was disabled during sampling. Bright spots in the plots represent locations in which a transition cell was active, and each plot is smoothed with a gaussian filter. This sampling method is used for all models, although the number of samplings per position depended on noise levels.

The standard model with parameters outlined in table 3.1, two models with similar parameters but different spatial input distributions (blue noise and white noise distributions, see figure 2.3), two models with a larger transition neuron network (23 and 37 cells), a model with minimal inhibitory delay (0.2 ms, but referred to as 'no delay', see section 2.3) and three models with added input noise.

Input noise occurred in the phase-delay of the input. Each theta cycle, each input had an expected delay depending on its spatial relevance relative to the animal's current position. The actual delay was modelled as normally distributed around this delay, with standard deviations of 1, 2 or 4 ms. All maintained a 20 ms temporal window each theta cycle.

The tenth model is a multi-compartment model with parameters similar to the standard model, referred to as the MC Model (see section 2.5). This model also used place-like inputs, but these inputs synapsed on non-spiking dendrites, each dendrite only receiving inputs from one input cell, and each dendrite subsequently affecting a single transition cell's spiking in a gap-junction-inspired way.

Each of the ten models was tested in 30 simulations on the same trajectory, and sampled every five minutes across the 95-minute simulation. Figure 3.2 shows a randomly chosen 95th minute sample from each model, showing that each model produced isolated firing fields, but not necessarily high levels of gridness.

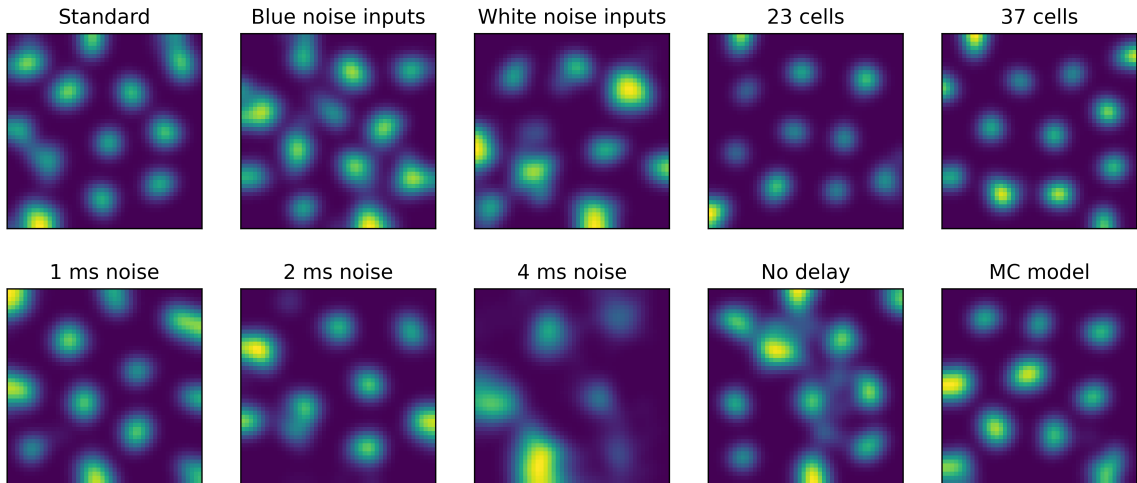


Figure 3.2: Example spike histograms sampled after 95 minutes simulated time for all ten models compared in this work. Notice that although not all models are equally gridlike, all show clearly isolated firing fields, as predicted from a STDP center-surround learning rule.

### 3.2 Gridness scores in the different models

The central question to this work was whether the network structure and learning rule described in the methods section could produce transition cells with a hexagonal firing patterns, which can be quantified by the gridness score. This gridness score was always computed on spike plots such as those shown in figure 3.1. Figure 3.3 (a) shows final mean gridness scores for each simulation after 95 simulated minutes, grouped by model, while figures 3.3 (b)-(e) show the temporal development of gridness scores in the ten models sorted in groups.

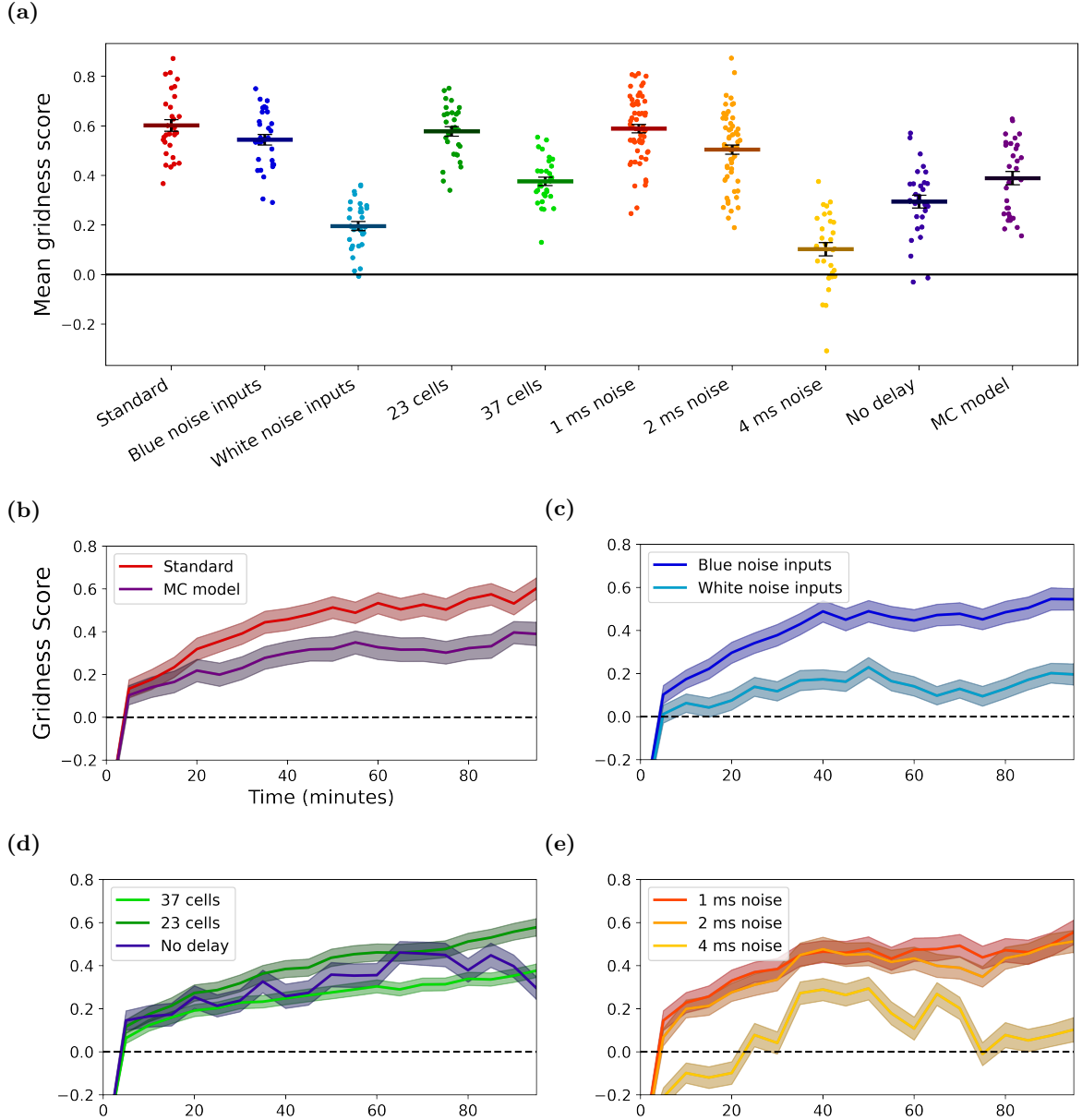


Figure 3.3: Gridness scores for ten model types. (a) Each scatter point represents mean gridness in one simulation after 95 minutes simulated time. Bars are means across all simulations for one type. (b-e) Loosely grouping the model types into four or five main categories. Colors are maintained from (a), with shaded region being 95 % confidence intervals. (b) The multi-compartment (MC) model shares many parameters with the standard model; they both have networks of 13 transition cells, no input noise and rectangularly spaced inputs. The standard model outperforms the MC Model, but both show clear gridness. (c) Models receiving inputs from a blue noise distribution have approximately equal gridness to the standard model, while transition cell networks receiving white-noise inputs do not see development. (d) Transition cells exhibit clear gridness both with minimal inhibitory delay and with different network sizes. While a network of 23 transition cells see the same gridness as the standard model, 37 transition cells have a somewhat reduced gridness. Without inhibitory delay, gridness is also reduced, and less stable. (e) While simulations with normally distributed input noise and std 1 or 2 ms have gridness comparable to the noiseless standard model, a std of 4 ms in input noise is not as robust.

While the standard model produced highest mean scores (0.60), multiple other configurations were comparable. Transition cell networks that received blue noise-distributed inputs (0.54), had 23 transition cells (0.57), or 1 ms noise (0.59) yielded similar gridness, and developed approximately equally quickly. The multi-compartment model also had high gridness (0.39), but lower than the

afore-mentioned groups, which was also the case for simulations with 37 transition cells (0.38), minimal inhibition delay (0.30) or 2 ms noise (0.50). Finally, white noise inputs performed worse (0.20), but was still significantly positive, while 4 ms input noise did not produce stable hexagonality (0.10).

Despite the differences in gridness, most cells across all simulations developed clear, isolated firing fields, and fired in multiple locations across the environment (see figure 3.2). To also have high gridness score, these firing fields should be bundled tightly to form hexagonal fields too, but not all models facilitated this.

In all models, within-simulation variance in gridness was high, and virtually all simulations had some cells with a negative gridness score at all times (figure 3.4). Low gridness scores can be explained by grid shearing or firing fields that aren't evenly distributed across the environment, while negative scores tend to reflect rectangularity.

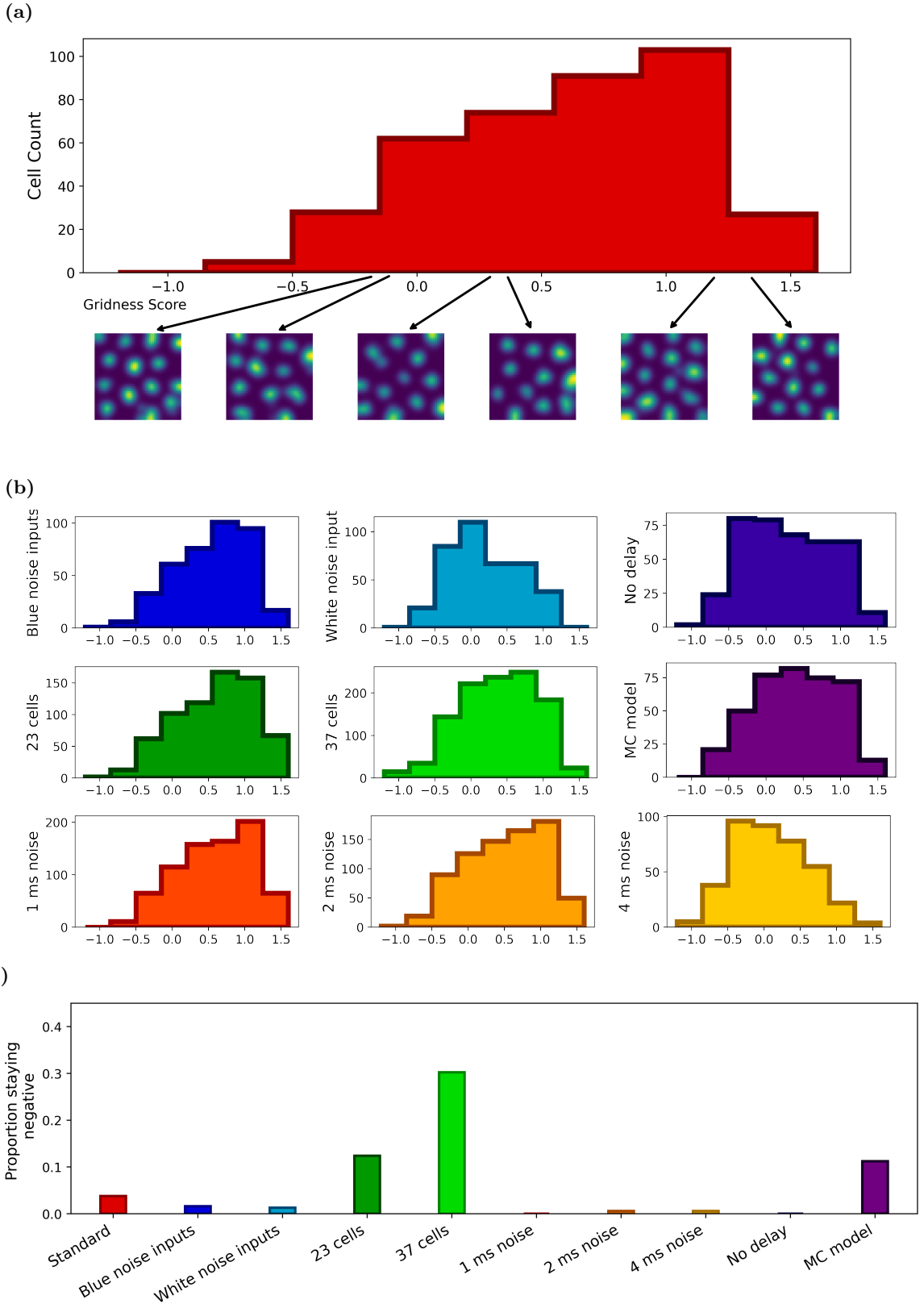


Figure 3.4: Distribution of gridness scores in the different models. (a) Standard model gridness distribution with spike plot examples. Although the mean gridness of this model is considered high (above 0.6), most simulated networks contain cells with negative or low gridness score. Negative gridness is typically produced by rectangular patterns, as shown in the two leftmost spikeplot examples. The two middle examples show activity in cells with positive, but low gridness scores. To have a gridness score above 1, the hexagonal pattern must typically span the whole environment without shearing or rectangularity. (b) Gridness score distributions for the remaining nine models. (c) Proportion of cells with negative final gridness score that also had negative gscore in all samples from the second half of the simulation. For most models, negative gridness was not maintained across the entire simulation.

Interestingly, the distributions of grid scores can also reflect features of models with lower gridness scores. The models with minimal inhibitory delay have a wide variety in gridness, so some cells are highly gridlike and others highly un-gridlike, while models with white noise inputs have a higher mode, but rarely sees highly hexagonal cells (see row 1, column 2 and 3 in figure 3.4 (b)). In the latter case, it is possible cells don't pack firing fields closely enough to develop high gridness, while in the former the between-transition cell competition might be too high to support large networks with high hexagonality.

Across models, a minority of cells with negative gridness at the last sample time had maintained negative scores across the final half of simulations (figure 3.4 (c)). This only exceeded chance levels of 5% in three models, the two with larger networks and the MC model. For most models, this means that there is some turnover in gridness, so at least some cells fluctuate between positive and negative scores over time. As demonstrated in section 3.5, this doesn't necessarily mean that the transition cell firing fields are unstable in time, and is instead taken as an indication that small changes to firing fields can impact gridness score significantly.

### 3.3 Orientation and phase distribution

According to experimental data, grid cells within a module align in orientation with a wall-angle offset of  $7.5^\circ$ , which was also observed in previous simulations of the TSS-model with related learning rules (Stensola et al. 2015; Waniek 2017). Grid cells with similar spacing and orientation should have phases that are evenly distributed on the toroidal manifold the network is active on, as seen in Gardner et al. 2022.

In this work, orientation was only computed for transition cells with positive gridness, and normalized to a value between  $0^\circ$  and  $60^\circ$ . Phase distribution was only computed on cells that aligned with the dominant orientation of that model so phase distribution could be accumulated across multiple simulations, and normalized to a position within a rhombus of the environment that correspond to the unwrapped torus.

In most simulations, the preferred orientation was around  $0^\circ$ , which indicates that transition cells align firing fields preferentially parallel to one of the environment walls (figure 3.5). However, this wasn't a strong preference, at most one in four cells with positive gridness showed this directionality. Models with noise had less of an orientation preference, and models with no inhibitory delay did not show any coorientation.

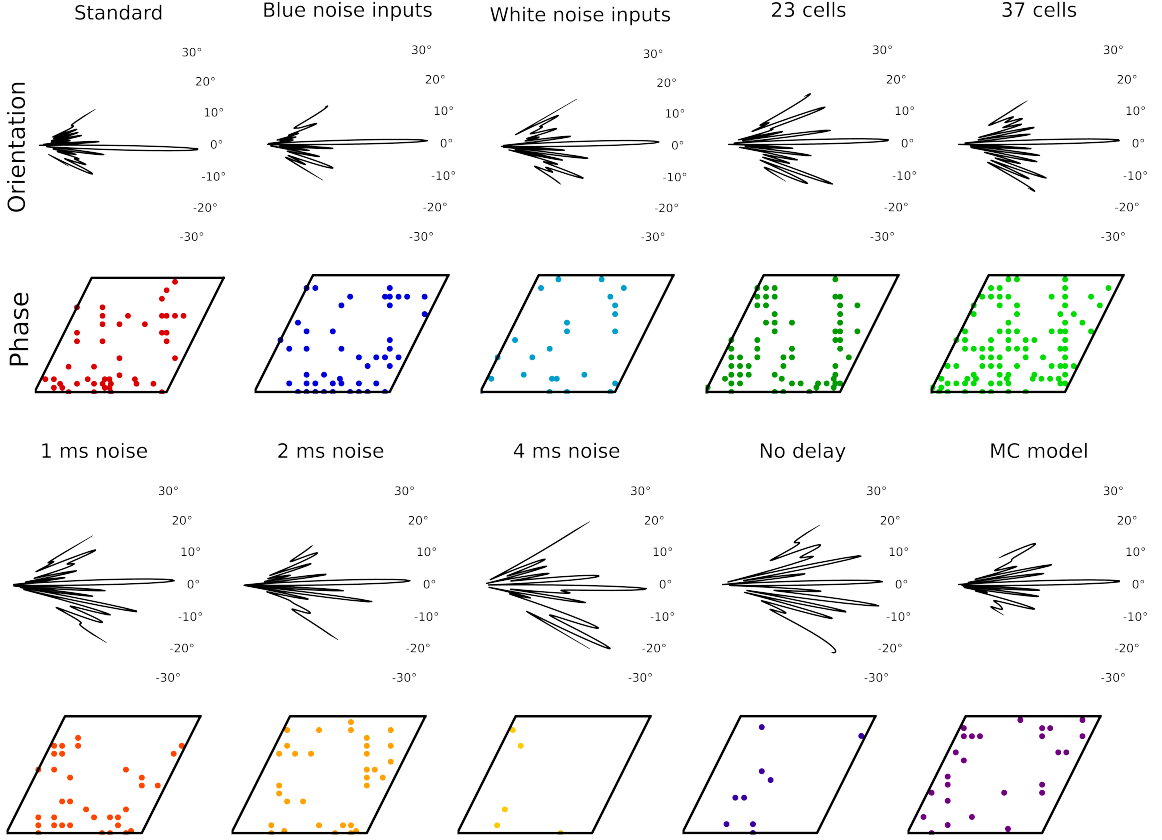


Figure 3.5: Orientations and phases of all models. Transition cells prefer a  $0^\circ$  orientation in most models (1st and 3rd row), exceptions being the minimal inhibitory delay model and the model with most input noise. The standard model and blue noise input distribution model have the strongest preference, while either increasing network size or adding noise reduces the preference. To compute phase distributions, only transition cells with positive gridness and an orientation between  $-5^\circ$  and  $5^\circ$  were considered. Within a simulation, one of the qualifying transition cells was chosen as a reference, and the dots show the other qualifying transition cells' phase relative to their reference (rows 2 and 4). This phase was computed as the offset of the peak relative to the center in the cross correlogram between the transition cell and the reference.

Too short simulated time for transition cells to develop the  $7.5^\circ$  orientation preference is one possibility, comparing with previous simulations, but based on 600 minute test simulations this was not the case.

Relative phase distribution can only be investigated in simulations with minimally two cells sharing orientation, preferably more, and this was more common in larger networks. In networks with 23 or 37 transition cells, the phases are evenly spread, without clear signs of clustering (figure 3.5 column 4 and 5 row 1). Computing phases was limited by the spatial resolution of the activity sampling, leading to rounded values.

It was briefly checked if the 37-cell networks had a toroidal structure in the population activity, which would be expected for grid cells belonging to the same module. Persistent cohomology was not observed in the populations, showing that the network probably does not align with structured population activity. It should be noted that those methods are developed for significantly larger networks, higher temporal resolution and rate-based network activity. However, it was considered unlikely that networks with at most a third of the cells sharing orientation would have a highly structured population activity, so this analysis was not pursued heavily.

### 3.4 Gridness spacing

All ten models introduced in section 3.1 used, barring noise, the same threshold for which spatial inputs would activate in a given location. Given a STDP-learning rule that lets an active transition cell decorrelate from less relevant spatial inputs, it would be expected that this relevance threshold is critical for the size of transition cell firing fields. That does not, however, mean that all models would give transition cells with the same spacing.

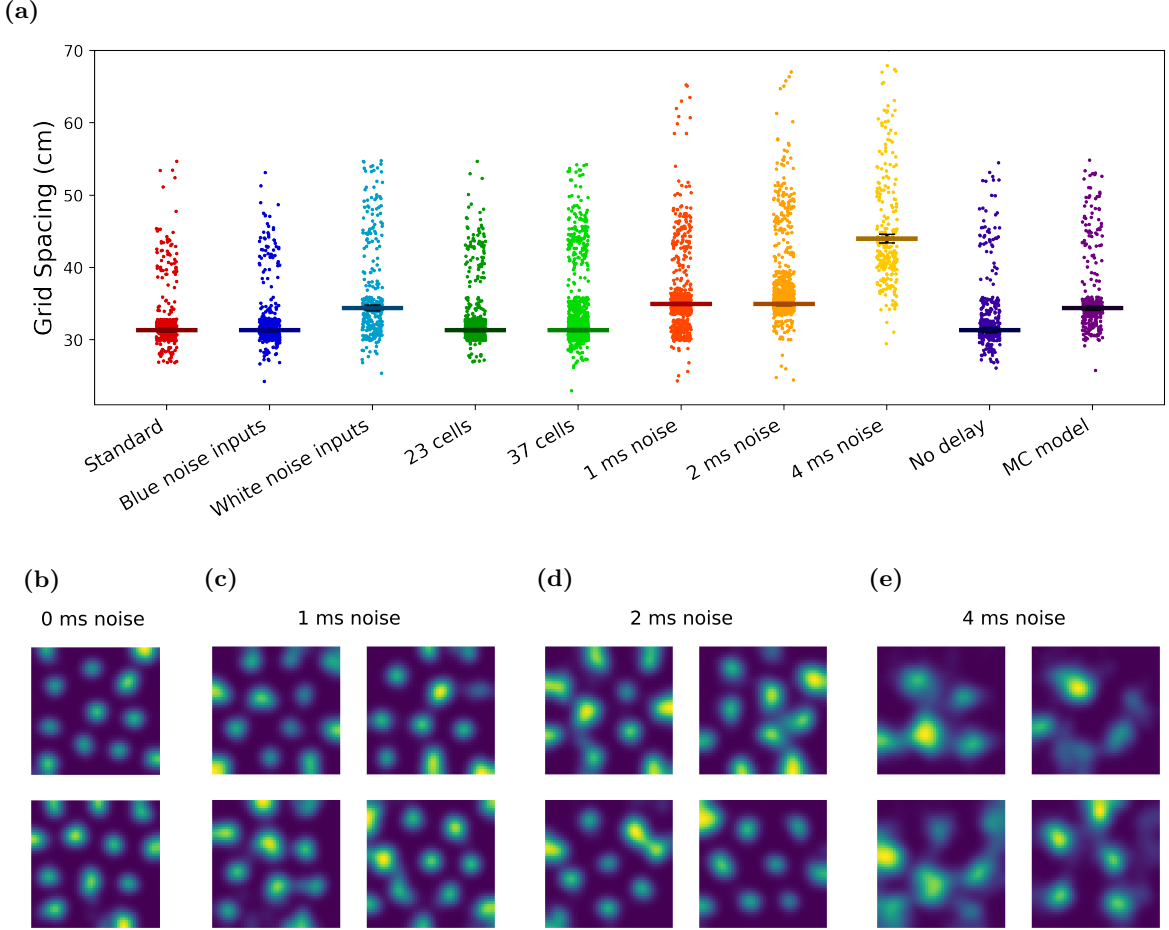


Figure 3.6: Grid spacing across ten models. This was computed as the spacing giving maximal gridness score for each cell after 95 simulated minutes. This was then filtered for cells with positive gridness. (a) Each dot represents the spacing in a single transition cell, sorted by model. Horizontal lines are model medians: for many models, the density is significantly higher close to the median than around. Notably, while mean spacing is invariant on network size, adding noise increases median spacing. Models with white noise inputs also had increased spacing, but poor gridness overall would make this measure less robust. Moreover, the multi-compartment model had higher spacing than the standard model. (b - e) Spike plots of models with identical parameters apart from input noise. (b) The standard model, without input noise, has a mean spacing of about 32.5 cm. As opposed to models with noise, transition cells can fit four firing fields horizontally in a 1 x 1 environment (lower spikeplot). (c & d) Models with 1 ms and 2 ms input noise have approximately similar mean spacing, at about 35 cm. (e) While 4 ms noise doesn't produce high gridness or clean firing fields, the average spacing is significantly larger than other models, with mean around 50 cm.

Curiously, while most models had highly similar spacing, which could be independent of input distribution and size of the transition cell layer (around 31.3 cm spacings), adding noise increased spacing, and it depended on amount of noise (figure 3.6). This was especially true for the highest noise level tested, with median spacing at 44 cm, while the 1 ms and 2 ms models had an approximately 35 cm spacing preference.

### 3.5 Temporal stability

Results from section 3.2 demonstrate that transition cells in many of the networks develop gridness, getting progressively more hexagonal with time(figure 3.3). However, it is unclear if the fields converge on some stable configuration, or if they continuously shift throughout the simulation. Under the TSS model, transition cells with incremental, gradually improving hexagonality is beneficial over transition cells with eratically changing fields, because transition cells also interconnect with place cells. Big changes in transition cell area will necessitate accurate changes in the connectivity between transition cells and place cells, increasing the likelihood of erroneous connections.

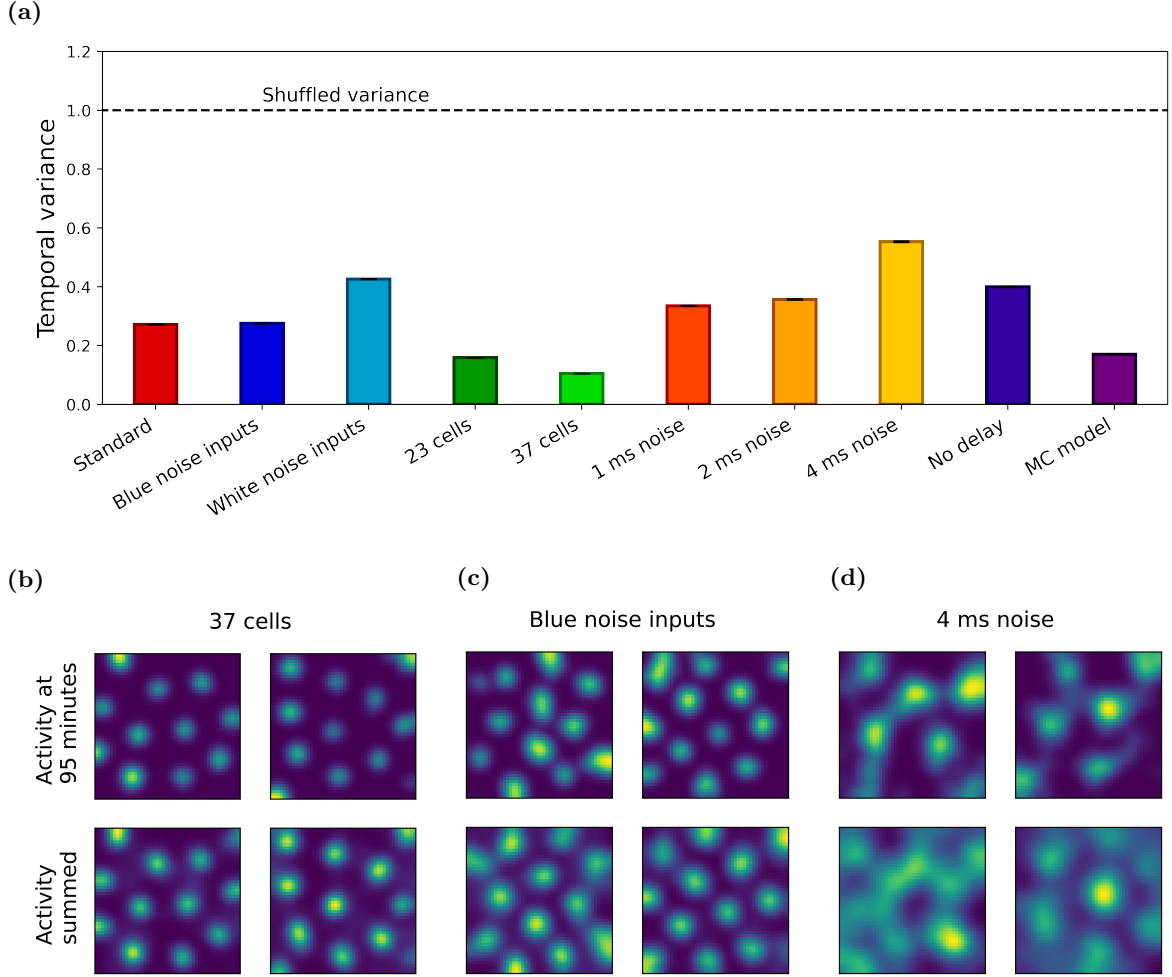


Figure 3.7: Temporal stability of different models. (a) The measure used to quantify temporal variance was the mean variance in spiking activity from one sampled time to the next, normalized by the variance in the shuffled data. A one in this score would indicate that there is no linear correlation between spiking from one sample time to the next, five simulated minutes later, while values close to zero indicate a positive correlation. Input noise decreases temporal stability, while inhibitory delay increases it. Larger networks also show more resistance to change. (b - d) The 95 minute sample activity (row 1) and summed activity over all sample times (row 2) for two cells each of three different models. All three models have clearly defined regions of activity and inactivity in their 95th minute sample. The summed activity, however, shows that transition cells in the 37 transition cell model and the blue noise input distribution model have maintained firing fields over time, while the noise model has not. This is reflected in their corresponding temporal variance scores.

To investigate this, a measure for temporal stability was used which tracks the transition cell activity in each of the sampled locations over time (figure 3.7 (a)). The measure is a temporal

correlation, in which the variance from one sample to the next, taken five simulation minutes later, is compared to the variance with shuffled data. This shuffled variance is used as a standard for no correlation, so a variance between 0 and 1 represents a positive temporal correlation, and variances above one is a negative correlation.

A positive correlation is clearly expected, because the input weights at one sampling time will be correlated to input weights at the next sampling. Additionally, the STDP learning rule is expected to encourage a cell to associate to some place and keep firing there. As such, the measure doesn't clearly indicate what should be understood as high temporal stability. Looking at spike plots instead, showing mean firing rates in each sampled location over time, shows a clear difference between models with low and high temporal stability (figures 3.7 (b) - (d)). Two randomly picked cells from three different models were chosen: the 37 transition cell model, which had the highest recorded stability, the 4 ms noise model with the lowest stability and the blue noise input distribution model as an intermediate one. The first row in each plot shows the activity at the final sampled time, 95 minutes, while the second row shows the summarized activity over all times. The 4 ms noise model shows comparably homogenous summed activity relative to the single-time sample, which is expected of models with low temporal stability. The other two models, on the other hand, show clearly peaked summed activity. This is taken as an indication that these models, and models with comparable spatial stability, produce transition cells that maintain their firing fields over time, and can represent spatial transitions stably.

Temporal stability is correlated with prolonged negative gridness (see figure 3.4 (c)). Despite the perceived benefit of temporal stability, it also indicates a lack of flexibility in converging on hexagonal firing fields.

### 3.6 Boundary Vector Cell Inputs

One goal of this work was to investigate the nature of spatial inputs. While previous sections describes how transition cells can obtain hexagonal activity with place cell-like inputs, the TSS model proposes that this input is conveyed to the transition cell soma through active computation in a dendritic tree (Waniek 2020). The spatial inputs given to this dendritic tree could have some other form, such as boundary vectors. Here, the dendritic tree is modelled as a multi-compartment model in which dendrites act as perceptrons, receiving some input and activating according to a softmax function to influence the transition cell body.

The only model that has been presented so far in doing this was a highly simplified version, in which the spatial input was rectangularly distributed and place cell-like, and the dendritic layer was simply conveying this information directly to the soma in a non-spiking manner, as a proof of concept. This model performs similarly to the standard model, but lacks a little in gridness (sections 3.2 - 3.5). An obstacle is that the addition of this intermediate dendrite layer increases simulation times significantly, so getting the right spiking dynamics as outlined in 3.1 is slow.

Further effort was made to move from this to a model taking boundary vector cell inputs. If dendrites should take BVC-inputs and convert them to place-like activity regions, this should be done in accordance to the previous results. Most importantly, if each dendrite responds to a single,

random location independent of all other dendrites, the resulting dendritic tree would presumably have a white-noise-like input distribution, which has been suboptimal in previous simulations.

With this in mind, the simplest BVC-model tried to replicate the rectangularly spaced inputs, so each dendrite received only two, orthogonal BVCs carefully tiled so each dendrite responds highly to a single position in a rectangular grid (figure 3.8 (a) & (b)). With this dual input, the dendrite stepwise activity would activate strongly when the input timing coincides, favoring places where both BVCs are equally far from their favored firing activity (figure 3.8 (c)). This gave dendrites a diagonal cross-like firing field, which is different from the firing fields used in dendrites in the MC model.

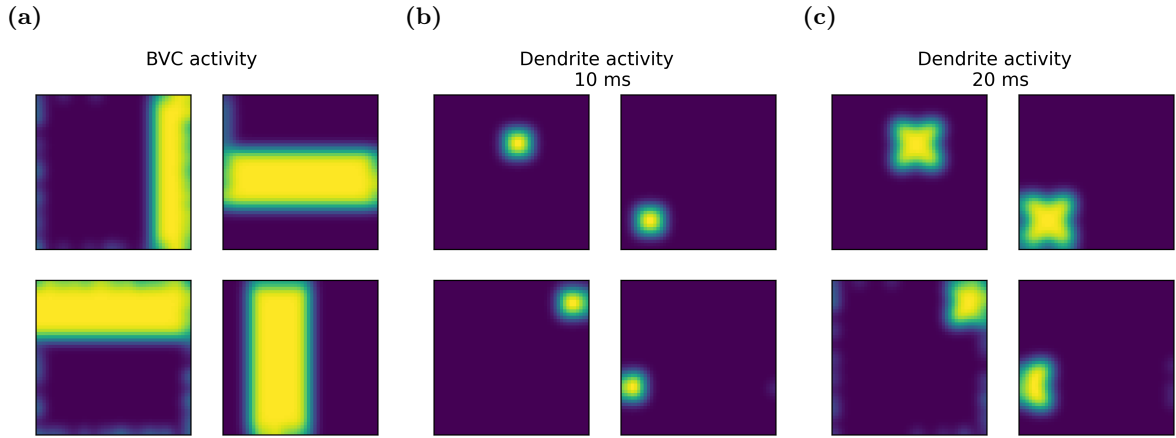


Figure 3.8: Boundary vector cell- and dendrite example activity during sampling. (a) In this model, all BVCs will align in one of the cardinal directions, giving them firing fields parallel to either the north/south walls or east/west walls. Distances were spaced linearly across the BVC population. (b) Dendrites would have an approximately circular firing fields at the intersection of their two input BVCs, if activity was limited to the first 10 ms of each theta cycle. (c) Across the entire time window, dendrites would activate in corners diagonal to their center of firing, places where their inputs would coincide late in the input window. This limits the similarity between this model and the models described in previous sections.

Next to the place-preference of each dendrites in this model, an advantage is that the state of the network can be directly read out from the dendrite-to-transition cell weights, or their conductances, as it is known at the start of a simulation which dendrite should respond to which place (figure 3.9 (b)). Although this model didn't develop overall positive gridness in test simulations, it did give transition cells with clear spatial firing fields (figure 3.9 (a)). Although this does not allow definitive conclusions on BVC as possible input structure, this shows some promise for this kind of model.

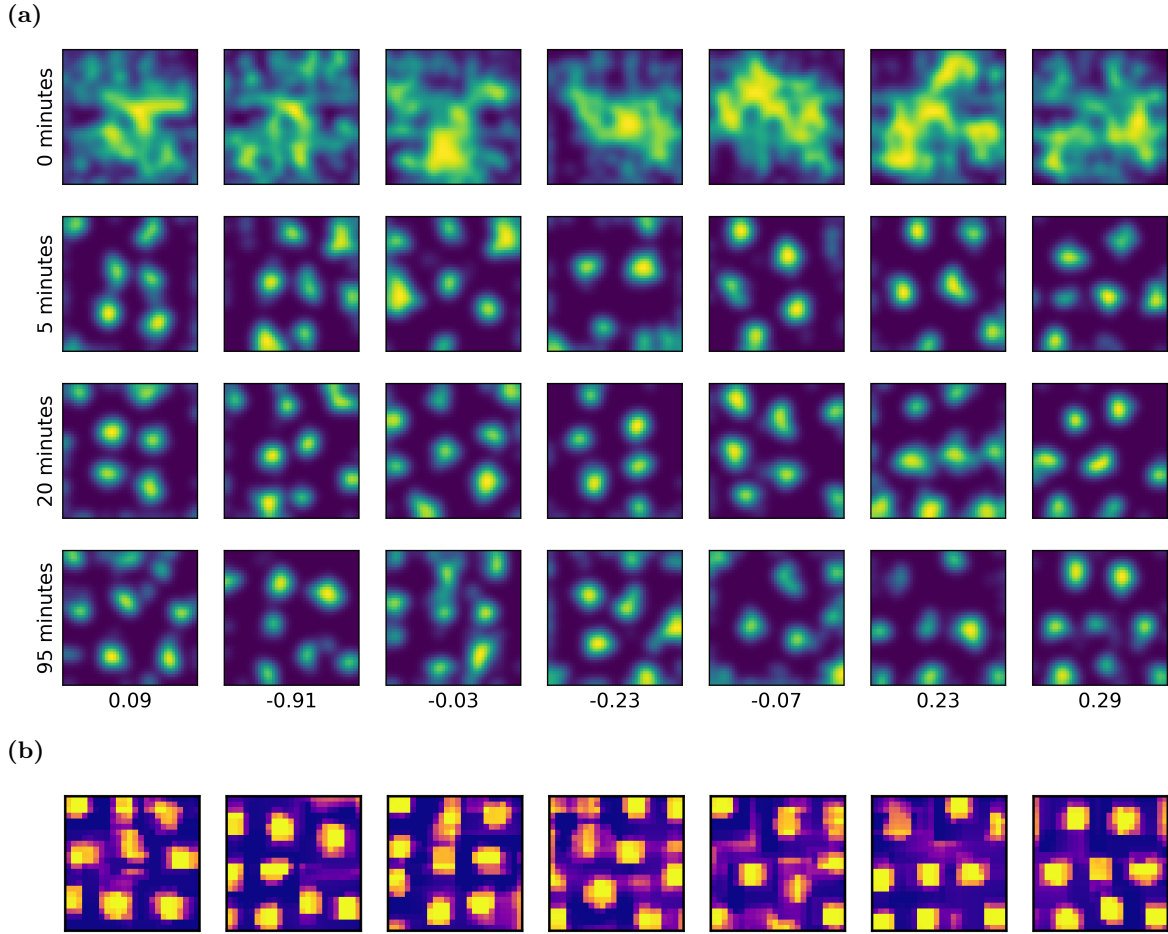


Figure 3.9: Preliminary results from a simplified BVC-model (a) Time series of sampled spike plots. Although the development of hexagonality isn't convincing, there are spatially separated firing fields. Each transition cell receives inputs from  $24 \times 24$  dendrites, similar to the MC Model, but these dendrites receive input from a pair of orthogonal BVCs. Values below final row are gridness scores of the corresponding firing histogram. (b) Dendrite-to-transition cell conductances from the bottom row in (a), sorted so each dendrite is placed in the intersection between the preferred firing fields of its two input BVCs.

## 4 Discussion

### 4.1 What this model shows

An ideal network was outlined in section 2.1, which defined what in this work is considered as biologically plausible. The concept of biologically plausible is vague, and in this work it refers to a series of requirements that, if broken, would suggest that the network depends on mechanisms that are not possible in a living neural network. Instantaneous inhibition is implausible, as is a learning rule that depends on variables that are not immediately available to the entity that undergoes learning. Spatial inputs that depend on past exploration are unlikely in a first environment encounter, and if the network breaks from too much noise, which is a given in a biological setting, this is also a sign that a living brain can't implement it.

Although the models presented in this work did not address all of these, mainly referring to the plausibility of spatial inputs, the simplified versions have made strides to address outstanding questions in the TSS-model. Compared to the upper limit of three transition cells seen in previous simulations (Waniek 2017), this work shed light on what is necessary to support bigger networks. Inhibition is considered an important feature of the network, because it prevents all cells from firing in all locations, but too strong inhibition leads to a competition in the network that prevents full crystallization of the transition cells. Possibly, this was both seen in the model with minimal inhibitory delay, that struggled to both coorient and develop high gridness, and in the network with 37 cells. The latter, which both showed high levels of coorientation, even phase distribution and high temporal stability, might have had too short of an inhibitory delay reflected in the increased competition of larger networks.

With this in mind, 37 cells is not considered an upper limit to these networks. Section 4.3 will go into the role of parameters and model testing, but a general observation is that parameter interactions makes scaling up network size and keeping everything else the same unlikely to work.

The two learning rules that competed to learn transitions were both biologically plausible and in line with the TSS model. Upon receiving dense spatial inputs, STDP promoted firing in separated fields, and baseline was included to encourage packing fields densely. These rules are online and local, but also lets transition cells relate to spatial inputs from the entire environment, which is necessary to encode transitions optimally.

Existing simulations of the TSS model had a third learning rule, an interaction rule, in which transition cells dissociated from spatial information whenever another transition cell activated first (Waniek 2017). This learning rule was not applied here because the implementation was unclear - one plausible alternative is that receiving inhibition would decrease weights, but this was technically difficult to implement with the simulation library used, and would have increased simulation times significantly.

While an interaction learning rule could encourage faster convergence and a wall-angle orientation closer to the grid cell 7.5° offset, as in the simulations that used it, this learning rule probably also increases competition. This work demonstrates that the interaction rule is not critical for gridness, and in order to avoid the increased competition, alternatives are discussed in section 4.5.

With regards to noise, the models here did prove reasonably resilient. Both models with 1 ms and 2 ms standard deviation on input noise within the 20 ms input window developed high gridness, and showed more similarities with the noiseless standard model than dissimilarities. Although this is taken as a positive indication, the striking decline in gridness in the model with 4 ms standard deviation shows that there might be some upperlimit. An interesting observation is that noise increased grid spacings, and with a large margin from 2 to 4 ms std dev. This work did not test grid cell size, but this, as well as the 4 ms noise model's seeming struggle to develop clear firing fields, can help explain why it didn't produce hexagonal gridness.

Considering the precision of BVC-activity using optic flow (Raudies and Hasselmo 2012), this network might have the necessary robustness against input noise. However, the noise models only evaluated noise in place-cell like inputs, which should be considered highly different from BVC noise. The BVC-models in this work assumed that each BVC was unique, so noise in BVC-inputs would impact a series of dendrites. Robustness to noise should be reevaluated in subsequent implementations with BVC-inputs, to see how this impacts the transition cells.

Looking away from the distribution of inputs, this work makes an argument that biological neural networks can create transition neurons as they are currently described in TSS. This is a significant result, because it implies that if spatial transitions are encoded in a brain network, it could very well be made out of transition cells with hexagonal firing fields. However, as the next section will describe, some predictions can be made about the spatial inputs these transition cells would need to receive to learn spatial transitions effectively.

## 4.2 Biological plausibility of input distributions and multi-compartment models

Since optic flow can explain boundary vector cell activity from pure visual inputs (Raudies and Hasselmo 2012), a network producing gridlike cells from BVC-inputs is desirable because it explains how spatial transitions can be learnt from sensory information available at the time of exploration. Under certain conditions, this network can be extrapolated to other vector-based inputs, such as object-vector cells, given that these cells can also be modeled from optic flow and that there is a sufficient number of environmental landmarks to triangulate positional information from. This doesn't mean that BVC inputs are necessary for transition cells, especially considering that it hasn't been observed in the brain, but this work does indicate that it is possible, and provides predictions for how BVCs can underlie transition cell activity.

Importantly, because most BVCs will be active in both center- and the surround regions of the transition cell (see section 2.2 and figure 3.8 (a)), linear summation of all boundary vector cell activity is unlikely to yield effective transition cells. Instead, some nonlinear process is necessary to allow transition cells to respond to BVCs in some locations, and not in others. In this work, the mechanism that supports this is dendritic computations, in which each dendrite receives a subset of BVC-inputs, and the transition cell in practice can learn on each dendrite, instead of individual inputs. This idea followed both experimental data on superlinear activation of pyramidal grid cell dendrites (Schmidt-Hieber et al. 2017), as well as a model using dendritic computations to explain

place cell remapping (Alabi, Vanderelst, and Minai 2000). In the model proposed in that article, each dendrite adapted to some place in some environment, and context-signals would inhibit all dendrites except the one governing the current environment. This allowed the place cell to remap orthogonally.

Using the same idea in this work, so each dendrite would represent some location in the environment, the learning variable was the dendrite conductance, and not synaptic weights. This isn't grounded in experimental observations, but rather because it contributed to model interpretability in two ways: first, that this mimics models in which place-like spatial inputs synapse onto grid cells, such as the other models in this work. This simplifies model comparisons, because the learning variable always has the same functional role in the network, as place-input to grid-cell weights. Secondly, although not directly explored here, one way of self-organizing BVC- to dendrite-connectivity is by randomly connecting a superfluous number of BVCs on each dendrite, and pruning unnecessary connections so the dendrite activates in only one or a few places. Differentiating between these two kinds of learning - BVC-to-dendrite and dendrite-to-grid cell, was thought to make these processes easier to distinguish. This model provides the testable hypothesis that 1) dendrites of either stellate or pyramidal mECII grid cells will exhibit place-like activity fields during traversal of familiar environments, and 2) only depolarization in certain grid cell dendrites, those responding to places within one of the firing fields of the grid cell, contribute to somatic depolarization and grid cell spiking.

That being said, while learning can occur in dendrite-to-grid cell conductances, these models don't depend on it. Alternatively, the STDP-learning signal must be transmitted to all postsynapses in the dendrite, in which all the BVC-to-dendrite weights will be changed indiscriminately, except possibly those pruned by mechanisms described in the above paragraph. In this case, it is also possible that all dendrites adapt place fields within the grid pattern in a given environment.

One of the most direct predictions from this work is that in the case of such a dendritic input tree, the distribution of place-like inputs to the grid cell should be relatively evenly distributed spatially. Using LIF neurons, convergence on hexagonal activity does not happen robustly with uniformly and independently distributed inputs (see figure 3.3 (a) and (c)). Blue noise patterns have a more even spread across the environment (figure 2.3), and this kind of distribution is biologically viable, having been observed for instance in the layout of cones in the human retina (Yellott 1983). However, making dendrites activate in a blue noise pattern would require some mechanism, for instance by making them disassociate from each other.

Further challenges underlie the model relying on an expansive dendritic tree as a hidden layer between vectorized inputs and grid-like transition cells. Not only is the number of dendrites quite high compared to both stellate and pyramidal principal mECII cells (Klink and Alonso 1998), but if each dendrite should correspond to one location, the required number of dendrites required would need to scale linearly with the number of places visited. If inspiration is again taken from what is known of hippocampal place cells, some kind of context modulation or remapping can help explain this, but significant work is required to highlight how this would work. With BVC-input, the same dendrite would in principle respond to the same place in multiple environments, as long as the boundary information is similar, so each dendrite could be reused across contexts. However, this

could require modulation of conductances across environments so one dendrite is varyingly active or inactive from one context to the next.

In sum, for the BVC model presented here to be biologically plausible, dendrites must learn to respond to single places in an environment, and across the dendritic tree, places should be evenly distributed. To support this, the transition cell needs to both learn to associate or dissociate from an entire dendrite, as well as having the dendrite associate or dissociate from singular BVCs to avoid chaotic activation across the environment. Then, plausibly, some mechanism should exist to let dendrites be reused across environments, for instance by modulating the grid cell's association to different dendrites across environments, inspired by (Alabi, Vanderelst, and Minai 2000). On a theoretical level, it might be necessary to map the computational limit of a finite dendritic tree, and how inputs would be used most effectively to let a transition cell cover as much area as possible. Biologically, this model hinges on the transition cell's ability to associate and dissociate to entire dendrites, for instance by opening or closing the dendrite radius to alter conductivity. Next to modelling work, this can be helpful in determining the computational power of biological neurons.

### 4.3 A word about parameters

As has been alluded to frequently throughout this work, simulating neural networks, and maybe particularly spiking neural networks, includes setting numerous parameters (see table 3.1). Understanding what each parameter does is a tall order, considering their numerous interactions, which was for instance shown when networks with minimal inhibitory delay gave positive results, counter to previous observations. Tuning hyperparameters to make learning rules that balance the incrementation and decreasing of weights required time and experimentation - in many networks, activity would fizzle out due to an overreactive dissociation. Coincidentally, when testing input networks of size 24x24 instead of 48x48 to reduce simulation times, mean gridness increased significantly, probably because this interacted with other parameters. The spike threshold might have gotten more accurate, or the learning rule parameters would end up more balanced.

Typically, tuning parameters would initially occur by producing the dynamics described in section 3.1. Did the model transition cells develop center surround areas, were all cells active, but in different areas, and did they pick up activity at the other side of a surround-field? In multi-compartment models, 10 seconds of simulated time took between 60 and 90 seconds, making such tests time consuming.

After these properties were satisfactory, long simulations were run to check results. Performance was quantified by gridness scores, as well as visually looking at spike plots. The gridness score's fragility to shearing makes it difficult to use reliably. In addition to frequently seeing cells with densely packed fields but negative scores, some cells did not look particularly hexagonal, but still had high scores because of the score's dependence on autocorrelation. This is part of the reason why spike plots frequently accompanied quantitative analysis in section 3.

With this in mind, it is worthwhile to stress that the majority of the results shown here are based on relatively little experimentation with parameters. The model with white noise distributed inputs was more closely tested than the standard model and blue noise distributed input models,

because of the perceived convenience of completely unstructured inputs. The fact that this model didn't produce high gridness nonetheless, isn't a conclusive proof that it's impossible, but rather a sign that it's implausible - getting a transition cell network to achieve gridness is probably easier with more homogenous spatial input distributions.

This should influence how results from models like this are interpreted. Occam's razor suggests that simple models should be preferred. Spiking neural networks are hardly simple, because of the number of parameters, so a useful measure can instead be the range of parameters that show the wanted properties. This work doesn't track that quantitatively, but it does indicate that some network structures more easily achieves the dynamics in question than others.

#### 4.4 This model as an mEC grid cell model

Although, as described in section 4.1, the models described here is a step towards biological plausibility of the TSS, it also tracked variables used to assess mECII grid cells. Summarized, the model should meet the following criteria to be considered a good grid cell model: First, that the network structure and morphology is reminiscent to the observed grid cell networks in the medial entorhinal cortex (mECII). Secondly, that the activity pattern of the transition cells fit some criteria: most importantly that their firing was sufficiently hexagonal to pass as grid cells, and then that they have similar grid spacings, a  $7.5^\circ$  wall-angle offset, and are reasonably temporally stable. On a population level, the models should support arbitrarily large networks, uniformly distributed phases and a toroidal structure in the population activity. Finally, the spatial inputs given to grid cells should be reminiscent of possible spatial inputs in mEC, although this is not fully mapped.

The results and networks described here fits a majority of these requirements. The fast-acting, strongly inhibiting interneurons were biologically inspired (Couey et al. 2013; Buetfering, Allen, and Monyer 2014). It is not clear that grid cells get spatially modulated input that is phase coded based on its relevance, but the theta-oscillations seen in the mEC shows some evidence of rhythmic activity (Wilson 1978). Importantly, given place-like inputs, models produce transition cells with high levels of gridness, that share spacing across the population and show temporal stability (figures 3.3, 3.6 and 3.7). This is true for different network sizes, with 13, 23 or 37 transition cells, although gridness decreased in the latter.

Looking at single cell characteristics, there are two primary questions left open from the results: first, that very few simulations produced cells with unvaryingly high scores, instead often containing cells with low or even negative gridness. Second, that while transition cells partly coorganized with a single orientation, there was no preference for the empirically supported  $7.5^\circ$  wall angle offset. Instead, transition cells aligned preferably in line with the wall, and this preference wasn't strong (figures 3.4 and 3.5).

These observations were universal across models, and longer simulations did not indicate that it was a matter of slow convergence. Because of the universality, it might not just be a question of setting hyperparameters better, but instead a matter of missing elements to the networks. This has also been seen in other feedforward models, discussed in section 4.5.

The conclusion that the network structure in mEC probably differs from the one used here is

supported when looking at the population dynamics. While networks of 37 transition cells developed reasonable gridness, cooriented with a  $0^\circ$  wall-angle offset and had uniform phase distribution, there was no evidence of population activity structured on a toroidal manifold. Existing literature shows how population activity within a grid cell module should represent the animal's position on a twisted torus (Gardner et al. 2022). This isn't conclusive - the best simulation for this comparison would be a single 37-cell simulation in which ten cells had positive gridness and an approximate  $0^\circ$  wall-angle offset, while the methods used to investigate this, inspired by Gardner et al. 2022, are adapted to use hundreds of grid cells. Possibly, even bigger networks would provide clearer answers.

There is reason to think otherwise. The toroidal structure in population activity also shows that grid cells maintain firing fields relative to each other across environments. Of course, this wasn't tested explicitly in this work, but with uniformly distributed initial weights and non-discriminatory inhibition, there is no mechanism in the network that encourages this kind of coalignment.

To qualify as a good grid cell model, the features described here should probably be taken into investigation. Experimental data and topological analysis suggest that grid cells align strongly in modules, maintained across environments. Despite the qualities the models in this work show, it is unlikely that the mEC is well-represented by this network structure. The models' current simplicity is an argument in their favor, but there is work remaining in making the transition cell network coaligned in a single module, which is clearly the case in the mECII.

## 4.5 Comparison to existing grid cell models

Considering changes that could be made to this network, it might first be beneficial to compare this model to some of the numerous existing grid cell models. To the writer's knowledge, this is the first grid cell model using phase-coded spatial inputs, which links mECII grid cells to the theoretical transition cells of the TSS-model. From the perspective of TSS, phase coding the spatial relevance gives transition cell information about center- vs surround fields. The transition cell uses this information to divide the environment into regions it encodes transitions from, and regions it encodes transitions to. In terms of biological plausibility, phase coding aligns with spike timing dependent plasticity as a learning rule that has been experimentally seen in the brain.

A strength of the model is that it does not rely on normalizing spike rates across the cell population or using implausible learning rules such as backpropagation through time (BPTT), which can be found in other grid cell models (Kropff and Treves 2008; Sorcher et al. 2023). Integrating spike timing and phase coding into a learning rule is an advantage biological, continuous time networks have, and might be central in understanding the brain beyond artificial neural networks. That being said, the upstream structure producing phase-coded inputs to transition cells has not been seen in the rodent brain.

The grid cell model developed in this work is not a pure feedforward model, because of the lateral inhibition between transition cells, but it shares many features with other models in this group. The benefit of learning spatial information through association and dissociation to external sensory inputs, as feedforward networks tend to do, is that the grid cell activity is less sensitive to drift (Mulas, Waniek, and Conradt 2016). To some extent, this was reflected in the temporal

stability shown in this work.

However, grid cells in feedforward models have some typical characteristics that do not fit experimental data, and that is true for this model too. Firing rate adaptation models required ad-hoc implementations to make grid cells co-orient, using excitatory recurrent connectivity (Barry et al. 2006; Si and Treves 2013). Although the model presented in this work showed some degree of preferred orientation, altering lateral connectivity in a similar way might be necessary to strengthen this preference and align the cells with the theoretical  $7.5^\circ$  wall angle offset.

Similar to the model in this work, another feed-forward model produced highly hexagonal grid cells, but with a wide distribution of gridness scores within populations (Weber and Sprekeler 2018). Here, grid cells received both place-based excitatory and inhibitory networks, and associated to both during firing. In simulations where inhibitory place cells had a wider receptive field than excitatory place cells, this would provide a similar surround-annulus of inhibition surrounding center-areas of association. Shearing or rectangularity was also described as causes leading to lower scores, which shows an inability to properly condense center-surround areas into the hexagonal pattern. However, the fact that hexagonality occurs in most cells, considering the positive mean gridness, it is not the learning rule itself, but possibly gridness competition across the population that prevents all cells from firing hexagonally. This is somewhat supported by the distribution of the high-competition no-delay model, where reduced inhibition times lead to a high proportion of highly negative gridscores (see figure 3.4 (b)).

Both the wide distribution of gridness scores and the lack of a wall angle offset can be addressed by changing the lateral connectivity between transition cells in the network, for instance by changing the role of inhibition. A goal would be to implement these models in larger networks, comparable to the neural recordings in (Gardner et al. 2022), and investigate if structured inhibition can place population activity on a toroidal manifold. Examples would be to make transition cells inhibit other transition cells with varying strength, or with different inhibitory delays. Getting a toroidal population activity would presumably imply co-orientation, and possibly a narrower distribution of gridness because firing fields for different transition cells would correlate more strongly. Whether such networks would preserve mean gridness score and uniform phases remains to be seen.

Possibly, future simulations should take more inspiration from CAN networks. Before this, however, it might be interesting to investigate the union between the toroidal population structure and the current TSS model.

An implication of this lateral connectivity would be that the transition cell population is a continuous attractor network. One rationale for this, under TSS, is that increasing mean gridness would make transition cells encode more transitions, on average. Although this work implies that transition cells can bundle a high number of spatial transitions with the networks used here, it would be in line with the TSS model if simple changes to network connectivity would improve transition-bundling further. Finding a proper union between the toroidal manifold of the grid cell network and the transition cells of TSS might require theoretical work on how transition cells ideally should coorganize in networks.

## 4.6 mECII as home to transition cells

The mECII grid cell resembles an optimal transition cell, as outlined by the TSS model (Waniek 2020). The argument that a transition cell should execute its purpose optimally in the brain is a cornerstone of the model, because it provides an answer to why grid cells should be expected in evolved neural networks of navigating agents. This work resolved unanswered questions on the biological compatibility of TSS, in a network inspired by mECII. However, the central question of whether mECII grid cells actually bundle spatial transitions for retrieval during navigation deserves scrutiny.

The basis for this investigation should probably start with the toroidal activity structure of mECII, and the question of why such a structure would be beneficial for a population of transition cells. Currently, TSS does not provide a clear rationale for why transition cell modules should keep relative phases between environments. If structuring lateral inhibition like a CAN-network reduces grid score variability and provides toroidal population activity, this would be a rationale for a CAN-network under the current TSS model by making transition cells more effective. However, assuming that the quality of a transition cell module only lies in the hexagonality of its cells may make us overlook possible benefits of coalignment on a network level. For instance, it might ease grid realignment across environment borders or compartments on a population level, making pathplanning across environment borders easier. Processes like this have been observed in the mEC (Carpenter et al. 2015).

The intersection between TSS and the structured population activity is highly interesting, and this work provides models that can be expanded to accommodate this. However, the engineer-like approach that is easy to adapt when designing neural networks might be premature, if the computational and behavioral purpose of the toroidal structure should be understood.

## 5 Conclusion

In the process of exploring areas of biological implausibility in the Transition Scale-Space model, this work has demonstrated the power of biological neurons interacting in continuous time and space. A criticism of the TSS model was that its simulations were implemented with for instance instant inhibition and backpropagation-based navigation, which require computational resources that might not be available in the brain. Results from this work indicates that transition cells can learn receptive fields from place-like or boundary vector cell inputs using phase-coded activity, delayed inhibition and dendritic computation. Although these computational resources play established roles in the brain but not used in perceptrons in today's artificial neural networks. In parallel work, modifying delays was tested as a potential alternative to the backpropagation used in Dijkstra's algorithm.

While results are promising, there are multiple areas of further development. First is exploring how and why a transition cell population should activate on a toroidal manifold. Establishing the full link from BVCs to transition cells, not to say visual inputs to transition cells, would be central in continuing the work of establishing TSS transition cells in biological neural networks. Finally, there is a long way left to test if spike delay can provide the necessary information as a biological alternative to backpropagation.

## References

- Alabi, Adedapo, Dieter Vanderelst, and Ali A. Minai (2000). “Context-Dependent Spatial Representations in the Hippocampus using Place Cell Dendritic Computation”. In: *IEEE*. doi: [10.1109/IJCNN.2000.892401](https://doi.org/10.1109/IJCNN.2000.892401).
- Ambrosa, Ellen R., Brad E. Pfeiffer, and David J. Foster (2013). “Reverse Replay of Hippocampal Place Cells Is Uniquely Modulated by Changing Reward”. In: *Neuron* 91, pp. 1124–1136. doi: <http://dx.doi.org/10.1016/j.neuron.2016.07.047>.
- Anderson, Michael I. and Kathrun J. Jeffrey (2013). “Heterogenous Modulation of Place Cell Firing by Changes in Context”. In: *Journal of Neuroscience* 33, pp. 8827–8835. doi: <https://doi.org/10.1523/JNEUROSCI.23-26-08827.2003>.
- Arne Høydal, Øyvind et al. (2019). “Object-vector coding in the medial entorhinal cortex”. In: *Nature* 468, pp. 400 –404. doi: <https://doi.org/10.1038/s41586-019-1077-7>.
- Barry, Caswell et al. (Jan. 2006). “The Boundary Vector Cell Model of Place Cell Firing and Spatial Memory”. In: *Reviews in the Neurosciences* 17.1-2. ISSN: 0334-1763. doi: [10.1515/revneuro.2006.17.1-2.71](https://doi.org/10.1515/revneuro.2006.17.1-2.71). URL: <http://dx.doi.org/10.1515/revneuro.2006.17.1-2.71>.
- Bellec, Guillaume et al. (2020). “A solution to the learning dilemma for recurrent networks of spiking neurons”. In: *Nature Communications* 11. doi: <https://doi.org/10.1038/s41467-020-17236-y>.
- Boccara, Charlotte N et al. (July 2010). “Grid cells in pre- and parasubiculum”. In: *Nature* 466, pp. 987–994. doi: <https://doi.org/10.1038/nature09122>.
- Bonnevie, Tora et al. (Mar. 2013). “Grid cells require excitatory drive from the hippocampus”. In: *Nature Neuroscience*, pp. 309–317. doi: <https://doi.org/10.1038/nn.3311>.

- Brandon, Mark P., Julie Koenig, and Stefan Leutgeb (2014). “Parallel and convergent processing in grid cell, head-direction cell, boundary cell, and place cell networks”. In: *WIREs Cognitive Science* 5.2, pp. 207–219. DOI: <https://doi.org/10.1002/wcs.1272>. eprint: <https://wires.onlinelibrary.wiley.com/doi/pdf/10.1002/wcs.1272>. URL: <https://wires.onlinelibrary.wiley.com/doi/abs/10.1002/wcs.1272>.
- Brandon, Mark P. et al. (2011). “Reduction of Theta Rhythm Dissociates Grid Cell Spatial Periodicity from Directional Tuning”. In: *Science* 332.6029, pp. 595–599. DOI: [10.1126/science.1201652](https://doi.org/10.1126/science.1201652). eprint: <https://www.science.org/doi/pdf/10.1126/science.1201652>. URL: <https://www.science.org/doi/abs/10.1126/science.1201652>.
- Brun, Vegard H. et al. (2002). “Place cells and place recognition maintained by direct entorhinal-hippocampal circuitry”. In: *Science* 296, pp. 2243 –2246. DOI: [10.1126/science.1071089](https://doi.org/10.1126/science.1071089).
- Buetefring, Christina, Kevin Allen, and Hannah Monyer (May 2014). “Parvalbumin interneurons provide grid cell-driven recurrent inhibition in the medial entorhinal cortex”. In: *Nature Neuroscience*, pp. 710–718. DOI: <https://doi.org/10.1038/nn.3696>.
- Burgess, Neil, Caswell Barry, and John O’Keefe (2007). “An oscillatory interference model of grid cell firing”. In: *Hippocampus* 17.9, pp. 801–812. DOI: <https://doi.org/10.1002/hipo.20327>. eprint: <https://onlinelibrary.wiley.com/doi/pdf/10.1002/hipo.20327>. URL: <https://onlinelibrary.wiley.com/doi/abs/10.1002/hipo.20327>.
- Carpenter, Francis et al. (2015). “Grid Cells Form a Global Representation of Connected Environments”. In: *Current Biology* 25, pp. 1176 –1182. DOI: <http://dx.doi.org/10.1016/j.cub.2015.02.037>.
- Castro, Luisa and Paulo Aguiar (Apr. 2014). “A feedforward model for the formation of a grid field where spatial information is provided solely from place cells”. In: *Biological Cybernetics* 108, pp. 133–143. DOI: <https://doi.org/10.1007/s00422-013-0581-3>.
- Chen, Guifen et al. (2016). “Absence of Visual input Results in the Disruption of Grid Cell Firing in the Mouse”. In: *Current Biology* 26, pp. 2335–2342. DOI: <https://doi.org/10.1016/j.cub.2016.06.043>.
- Cherubini, Enrico and Richard Miles (2015). “The CA3 region of the hippocampus: how is it? what is it for? how does it do it?” In: *Frontiers in Cellular Neuroscience* 9. ISSN: 1662-5102. DOI: [10.3389/fncel.2015.00019](https://doi.org/10.3389/fncel.2015.00019). URL: <https://www.frontiersin.org/articles/10.3389/fncel.2015.00019>.
- Cheung, Allen et al. (2007). “Animal navigation: the difficulty of moving in a straight line”. In: *Biological Cybernetics* 97, pp. 47–61. DOI: <https://doi.org/10.1007/s00422-007-0158-0>.
- Christensen, Ane Charlotte et al. (Jan. 2021). “Perineuronal nets stabilize the grid cell network”. In: *Nature Communications*, p. 253. DOI: <https://doi.org/10.1038/s41467-020-20241-w>.
- Couey, Jonathan J et al. (Mar. 2013). “Recurrent inhibitory circuitry as a mechanism for grid formation”. In: *Nature Neuroscience*, pp. 318–324. DOI: <https://doi.org/10.1038/nn.3310>.
- Dong, Can, Antoine D. Madar, and Mark E. J. Sheffield (2021). “Distinct place cell dynamics in CA1 and CA3 encode experience in new environments”. In: *Nature communications* 12. DOI: <https://doi.org/10.1038/s41467-021-23260-3>.

- Dragoi, George and Susumu Tonegawa (Jan. 2011). “Preplay of future place cell sequences by hippocampal cellular assemblies”. In: *Nature* 469, pp. 397–401. DOI: <https://doi.org/10.1038/nature09633>.
- (May 2013). “Distinct preplay of multiple novel spatial experiences in the rat”. In: *PNAS*. DOI: <https://doi.org/10.1073/pnas.1306031110>.
- Dudchenko, Paul A. (2010). *Why People Get Lost: The Psychology and Neuroscience of Spatial Cognition*. Oxford: Oxford University Press. DOI: <https://doi.org/10.1093/acprof:oso/9780199210862.001.0001>.
- Etienne, Ariane S. et al. (1986). “Short-distance homing in the golden hamster after a passive outward journey”. In: *Animal Behaviour* 34, pp. 696 –715. DOI: [https://doi.org/10.1016/S0003-3472\(86\)80054-9](https://doi.org/10.1016/S0003-3472(86)80054-9).
- Furtak, Sharon C. et al. (Aug. 2007). “Functional Neuroanatomy of the Parahippocampal Region in the Rat: The Perirhinal and Postrhinal Cortices”. In: *Hippocampus* 17, pp. 709 –722. DOI: <https://doi.org/10.1002/hipo.20314>.
- Fyhn, Marianne et al. (2007). “Hippocampal remapping and grid realignment in entorhinal cortex”. In: *Nature* 446, pp. 190 –194. DOI: <https://doi.org/10.1038/nature05601>.
- Gardner, Richard J. et al. (Feb. 2022). “Toroidal topology of population activity in grid cells”. In: *Nature*, pp. 123–128. DOI: <https://doi.org/10.1038/s41586-021-04268-7>.
- George, Tom M. et al. (2024). “RatInABox, a toolkit for modelling locomotion and neuronal activity in continuous environments”. In: *eLife* 13. DOI: <https://doi.org/10.7554/eLife.85274>.
- Groenand, Thomas van and J. Michael Wyss (June 1990). “The connections of presubiculum and parasubiculum in the rat”. In: *Brain Research* 518, pp. 227 –243. DOI: [https://doi.org/10.1016/0006-8993\(90\)90976-I](https://doi.org/10.1016/0006-8993(90)90976-I).
- Hafting, Torkel et al. (2008). “Hippocampus-independent phase precession in entorhinal grid cells”. In: *Nature* 453, pp. 1248–1252. DOI: <https://doi.org/10.1038/nature06957>.
- Hafting, Torkild et al. (Aug. 2005). “Microstructure of a spatial map in the entorhinal cortex”. In: *Nature*, pp. 801–806. DOI: <https://doi.org/10.1038/nature03721>.
- Hodgkin, A. L. and A. F. Huxley (1952). “A quantitative description of the membrane current and its application to conduction and excitation in the nerve”. In: *The Journal of Physiology* 4, pp. 500 –544. DOI: <https://doi.org/10.1113/jphysiol.1952.sp004764>.
- Kerr, Kristin M. et al. (Aug. 2007). “Functional Neuroanatomy of the Parahippocampal Region: The Lateral and Medial Entorhinal Areas”. In: *Hippocampus* 17, pp. 697 –708. DOI: <https://doi.org/10.1002/hipo.20315>.
- Kim, Soyun et al. (2013). “Contrasting effects on path integration after hippocampal damage in humans and rats”. In: *Proceedings of the National Academy of Sciences of the United States of America* 110, pp. 4732–4737. DOI: <https://doi.org/10.1073/pnas.1300869110>.
- Klink, Ruby and Angel Alonso (1998). “Morphological characteristics of layer II projection neurons in the rat medial entorhinal cortex”. In: *Hippocampus* 7, pp. 571–583. DOI: [https://doi.org/10.1002/\(SICI\)1098-1063\(1997\)7:5<571::AID-HIP012>3.0.CO;2-Y](https://doi.org/10.1002/(SICI)1098-1063(1997)7:5<571::AID-HIP012>3.0.CO;2-Y).

- Koenig, Julie et al. (2011). “The Spatial Periodicity of Grid Cells Is Not Sustained During Reduced Theta Oscillations”. In: *Science* 332.6029, pp. 592–595. DOI: 10.1126/science.1201685. eprint: <https://www.science.org/doi/pdf/10.1126/science.1201685>. URL: <https://www.science.org/doi/abs/10.1126/science.1201685>.
- Krichmar, Jeffrey L. et al. (2022). “Flexible Path Planning in a Spiking Model of Replay and Vicarious Trial and Error”. In: *From Animals to Animats* 16, pp. 177–189. DOI: [https://doi.org/10.1007/978-3-031-16770-6\\_15](https://doi.org/10.1007/978-3-031-16770-6_15).
- Kropff, Emilio and Alessandro Treves (2008). “The emergence of grid cells: Intelligent design or just adaptation?” In: *Hippocampus* 18.12, pp. 1256–1269. DOI: <https://doi.org/10.1002/hipo.20520>. eprint: <https://onlinelibrary.wiley.com/doi/pdf/10.1002/hipo.20520>. URL: <https://onlinelibrary.wiley.com/doi/abs/10.1002/hipo.20520>.
- Kropff, Emilio et al. (2015). “Speed cells in the medial entorhinal cortex”. In: *Nature* 523, pp. 419–424. DOI: <https://doi.org/10.1038/nature14622>.
- Krupic, Julija et al. (Feb. 2015). “Grid cell symmetry is shaped by environmental geometry”. In: *Nature*, pp. 232–235. DOI: <https://doi.org/10.1038/nature14153>.
- Kunsch, H.R., E. Agrell, and F.A. Hamprecht (2005). “Optimal lattices for sampling”. In: *IEEE Transactions on Information Theory* 51.2, pp. 634–647. DOI: 10.1109/TIT.2004.840864.
- Langston, Rosamund F. et al. (2010). “Development of the Spatial Representation System in the Rat”. In: *Science* 328.5985, pp. 1576–1580. DOI: 10.1126/science.1188210. eprint: <https://www.science.org/doi/pdf/10.1126/science.1188210>. URL: <https://www.science.org/doi/abs/10.1126/science.1188210>.
- Lever, Colin et al. (2009). “Boundary Vector Cells in the Subiculum of the Hippocampal Formation”. In: *The Journal of Neuroscience* 29, pp. 9771–9777. DOI: <https://doi.org/10.1523/JNEUROSCI.1319-09.2009>.
- Monsalve-Mercado, Mauro M. and Christian Leibold (Oct. 2020). “Effect of boundaries on grid cell patterns”. In: *Physiological Review Research* 2. DOI: <https://doi.org/10.1103/PhysRevResearch.2.043137>.
- Muessig, Laurenz et al. (Feb. 2024). “Environment geometry alters subiculum boundary vector cell receptive fields in adulthood and early development”. In: *Nature Communications* 15, p. 982. DOI: <https://doi.org/10.1038/s41467-024-45098-1>.
- Mulas, Marcello, Nicolai Waniek, and Jorg Conradt (2016). “Hebbian Plasticity Realigns Grid Cell Activity with External Sensory Cues in Continuous Attractor Models”. In: *Frontiers in Computational Neuroscience* 10. DOI: <https://doi.org/10.3389/fncom.2016.00013>.
- Muller, Robert U. and John L. Kubie (July 1987). “The Effects of Changes in the Environment on the Spatial Firing of Hippocampal Complex-Spike Cells”. In: *The Journal of Neuroscience* 7, pp. 1951–1968. DOI: <https://doi.org/10.1523/JNEUROSCI.07-07-01951.1987>.
- Niedermeier, Lars and Jeffrey L. Krichmar (2023). “Experience-Dependent Axonal Plasticity in Large-Scale Spiking Neural Network Simulations”. In: *IEEE*. DOI: 10.1109/IJCNN54540.2023.10191241.

- O'Keefe, John (1976). "Place units in the hippocampus of the freely moving rat". In: *Experimental Neurology* 51.1, pp. 78–109. ISSN: 0014-4886. DOI: [https://doi.org/10.1016/0014-4886\(76\)90055-8](https://doi.org/10.1016/0014-4886(76)90055-8). URL: <https://www.sciencedirect.com/science/article/pii/0014488676900558>.
- O'Keefe, John and Jonathan O. Dostrovsky (1976). "The hippocampus as a spatial map: Preliminary evidence from unit activity in the freely-moving rat." In: *Brain Research*, pp. 171–175. DOI: [https://doi.org/10.1016/0006-8993\(71\)90358-1](https://doi.org/10.1016/0006-8993(71)90358-1).
- O'Keefe, John and Michael L. Reese (July 1993). "Phase relationship between hippocampal place units and the EEG theta rhythm". In: *Hippocampus* 3 (3), pp. 317 –330. DOI: <https://doi.org/10.1002/hipo.450030307>.
- Olafsdottir, H Freyja, Francis Carpenter, and Caswell Barry (June 2016). "Coordinated grid and place cell replay during rest". In: *Nature Neuroscience*, pp. 792–794. DOI: <https://doi.org/10.1038/nrn.4291>.
- Raudies, Florian and Michael E. Hasselmo (June 2012). "Modeling Boundary Vector Cell Firing Given Optic Flow as a Cue". In: *PLOS Computational Biology* 8.6, pp. 1–17. DOI: [10.1371/journal.pcbi.1002553](https://doi.org/10.1371/journal.pcbi.1002553). URL: <https://doi.org/10.1371/journal.pcbi.1002553>.
- Rowland, David C et al. (Sept. 2018). "Functional properties of stellate cells in medial entorhinal cortex layer II". In: *eLife*. DOI: <https://doi.org/10.7554/eLife.36664>.
- Sargolini, Francesca et al. (2006). "Conjunctive Representation of Position, Direction, and Velocity in Entorhinal Cortex". In: *Science* 312, pp. 758 –762. DOI: [10.1126/science.1125572](https://doi.org/10.1126/science.1125572).
- Schmidt-Hieber, Christoph et al. (Aug. 2017). "Active dendritic integration as a mechanism for robust and precise grid cell firing". In: *Nature*, pp. 1114–1121. DOI: <https://doi.org/10.1038/nature23582>.
- Si, Bailu and Alessandro Treves (Aug. 2013). "A model for the differentiation between grid and conjunctive units in medial entorhinal cortex". In: *Hippocampus* 23, pp. 1410 –1424. DOI: <https://doi.org/10.1002/hipo.22194>.
- Skaggs, William E. et al. (1996). "Theta phase precession in hippocampal neuronal populations and the compression of temporal sequences". In: *Hippocampus* 6 (2), pp. 149–172. DOI: [https://doi.org/10.1002/\(SICI\)1098-1063\(1996\)6:2<149::AID-HIP06>3.0.CO;2-K](https://doi.org/10.1002/(SICI)1098-1063(1996)6:2<149::AID-HIP06>3.0.CO;2-K).
- Soldatkina, Oleksandra, Francesca Schonsberg, and Alessandro Treves (Oct. 2021). "Challenges for Place and Grid Cell Models". In: *Computational Modelling of the Brain* 1359, pp. 285 –312. DOI: <https://doi.org/10.1007/97>.
- Solstad, Trygve et al. (2008). "Representation of Geometric Borders in the Entorhinal Cortex". In: *Science* 322, pp. 1865 –1868. DOI: [10.1126/science.1166466](https://doi.org/10.1126/science.1166466).
- Song, Sen, Kenneth D. Miller, and L. F. Abbott (2000). "Competitive Hebbian learning through spike-timing-dependent synaptic plasticity". In: *Nature Neuroscience* 3, pp. 919 –926. DOI: <https://doi.org/10.1038/78829>.
- Sorcher, Ben et al. (2023). "A unified theory for the computational and mechanistic origins of grid cells". In: *Neuron* 111, pp. 121–137. DOI: <https://doi.org/10.1016/j.neuron.2022.10.003>.
- Stensola, Hanne et al. (Dec. 2012). "The entorhinal grid map is discretized". In: *Nature*, pp. 72 –78. DOI: <https://doi.org/10.1038/nature11649>.

- Stensola, Tor et al. (Feb. 2015). “Shearing-induced asymmetry in entorhinal grid cells”. In: *Nature*, pp. 207–212. DOI: <https://doi.org/10.1038/nature14151>.
- Stimberg, Marcel, Romain Brette, and Dan F. M. Goodman (2019). “Brian2, an intuitive and efficient neural simulator”. In: *eLife* 8. DOI: <https://doi.org/10.7554/eLife.47314>.
- Suzuki, Shinya, Gerda Augerinos, and Abraham H. Black (Feb. 1980). “Stimulus control of spatial behavior on the eight-arm maze in rats”. In: *Learning and Motivation* 11, pp. 1–18. DOI: [https://doi.org/10.1016/0023-9690\(80\)90018-1](https://doi.org/10.1016/0023-9690(80)90018-1).
- Tamamaki, Nobuaki and Yoshiaki Nojyo (Oct. 1993). “Projection of the entorhinal layer II neurons in the rat as revealed by intracellular pressure-injection of neurobiotin”. In: *Hippocampus* 3, pp. 471 –480. DOI: <https://doi.org/10.1002/hipo.450030408>.
- Taube, Jeffrey S. (2007). “The Head Direction Signal: Origins and Sensory-Motor Integration”. In: *Annual Review of Neuroscience* 30, pp. 181 –207. DOI: <https://doi.org/10.1146/annurev.neuro.29.051605.112854>.
- Taube, Jeffrey S., Robert U. Muller, and Jr. James B. Ranck (1990). “Head-Direction Cells Recorded from the Postsubiculum in Freely Moving Rats. I. Description and Quantitative Analysis”. In: *The Journal of Neuroscience* 10, pp. 420 –435. DOI: <https://doi.org/10.1523/JNEUROSCI.10-02-00420.1990>.
- Tolman, Edward C. (1948). “Cognitive Maps in Rats and Men”. In: *Psychological Review* (55), pp. 189 –208.
- Tolman, Edward C., B. F. Ritchie, and D. Kalish (1946). “Studies in Spatial Learning. I. Orientation and the Short-cut”. In: *Journal of Experimental Psychology* (36), p. 13. DOI: <https://doi.org/10.1037/h0053944>.
- Veen, Werner van der (2022). “Including STDP to eligibility propagation in multi-layer recurrent spiking neural networks”. In: *arxiv*. DOI: <https://doi.org/10.48550/arXiv.2201.07602>.
- Waniek, Nicolai (2017). “Multi-Transition Systems: A theory for neural spatial navigation”. In: *BioRxiv*. DOI: <https://doi.org/10.1101/174946>.
- (2018). “Hexagonal Grid Fields Optimally Encode Transitions in Spatiotemporal Sequences”. In: *Neural Computation* (30), pp. 2691–2725. DOI: [https://doi.org/10.1162/neco\\_a\\_01122](https://doi.org/10.1162/neco_a_01122).
- (2020). “Transition Scale-Spaces; A Computational Theory for the Discretized Entorhinal Cortex”. In: *Neural Computation* (32), pp. 330–394. DOI: [https://doi.org/10.1162/neco\\_a\\_01255](https://doi.org/10.1162/neco_a_01255).
- (2023). “An introduction to the Transition Scale-Space model for grid cells”. In: URL: <https://rochus.net/pdf/waniek2023tssintro.pdf>.
- Weber, Simon N. and Henning Sprekeler (Feb. 2018). “Learning place cells, grid cells and invariances with excitatory and inhibitory plasticity”. In: *eLife* 7. DOI: <https://doi.org/10.7554/eLife.34560>.
- Widloski, John and Ila R. Fiete (2014). “A Model of Grid Cell Development through Spatial Exploration and Spike Time-Dependent Plasticity”. In: *Neuron* 83.2, pp. 481–495. ISSN: 0896-6273. DOI: <https://doi.org/10.1016/j.neuron.2014.06.018>.

- Wills, Tom J., Caswell Barry, and Francesca Cacucci (2012). “The abrupt development of adult-like grid cell firing in the medial entorhinal cortex”. In: *Frontiers in Neural Circuits* 6. ISSN: 1662-5110. DOI: 10.3389/fncir.2012.00021. URL: <https://www.frontiersin.org/articles/10.3389/fncir.2012.00021>.
- Wills, Tom J. et al. (2010). “Development of the Hippocampal Cognitive Map in Preadolescent Rats”. In: *Science* 328.5985, pp. 1573–1576. DOI: 10.1126/science.1188224. eprint: <https://www.science.org/doi/pdf/10.1126/science.1188224>. URL: <https://www.science.org/doi/abs/10.1126/science.1188224>.
- Wilson, Jonathan (1978). “Loss of Hippocampal Theta Rhythm Results in Spatial Memory Deficit in the Rat”. In: *Science* 201, pp. 160–163. DOI: 10.1126/science.663646.
- Wilson, Matthew A. and Bruce L. McNaughton (1993). “Dynamics of the Hippocampal Ensemble Code for Space”. In: *Science* 261.5124, pp. 1055–1058. DOI: 10.1126/science.8351520. eprint: <https://www.science.org/doi/pdf/10.1126/science.8351520>. URL: <https://www.science.org/doi/abs/10.1126/science.8351520>.
- (1994). “Reactivation of Hippocampal Ensemble Memories During Sleep”. In: *Science* 265.5172, pp. 676–679. DOI: 10.1126/science.8036517. eprint: <https://www.science.org/doi/pdf/10.1126/science.8036517>. URL: <https://www.science.org/doi/abs/10.1126/science.8036517>.
- Witter, Menno P. et al. (2017). “Architecture of the Entorhinal Cortex A Review of Entorhinal Anatomy in Rodents with Some Comparative Notes”. In: *Frontiers in Systems Neuroscience* 11. DOI: <https://doi.org/10.3389/fnsys.2017.00046>.
- Wynn, Joe and Miriam Liedvogel (2023). “Lost: on what level should we aim to understand animal navigation?” In: *Journal of Experimental Biology* 226. DOI: <https://doi.org/10.1242/jeb.245441>.
- Yartsev, Michael M., Menno P. Witter, and Nachum Ulanovsky (Nov. 2011). “Grid cells without theta oscillations in the entorhinal cortex of bats”. In: *Nature* 479, pp. 103–107. DOI: <https://doi.org/10.1038/nature10583>.
- Yellott, John I. (1983). “Spectral Consequences of Photoreceptor Sampling in the Rhesus Retina”. In: *Science* 221, pp. 382–385. DOI: 10.1126/science.6867716.
- Yoon, KiJung et al. (July 2013). “Specific evidence of low-dimensional continuous attractor dynamics in grid cells”. In: *Nature Neuroscience* 16, pp. 1077–1084. DOI: <https://doi.org/10.1038/nn.3450>.
- Zilli, Eric (2012). “Models of Grid Cell Spatial Firing Published 2005–2011”. In: *Frontiers in Neural Circuits* 6. ISSN: 1662-5110. DOI: 10.3389/fncir.2012.00016. URL: <https://www.frontiersin.org/articles/10.3389/fncir.2012.00016>.
- Zilli, Eric A. and Michael E. Hasselmo (2010). “Coupled Noisy Spiking Neurons as Velocity-Controlled Oscillators in a Model of Grid Cell Spatial Firing”. In: *Journal of Neuroscience* 30.41, pp. 13850–13860. ISSN: 0270-6474. DOI: 10.1523/JNEUROSCI.0547-10.2010. eprint: <https://jneurosci.org/content/30/41/13850.full.pdf>. URL: <https://www.jneurosci.org/content/30/41/13850>.

## A Appendix: A navigation model

### A.1 Introduction

The TSS model suggests that a transition cell network encodes spatial transitions, which can be used to produce place cell sequences. This has been tested in simulations (Waniek 2020), but these simulations used Dijkstra’s method to produce the sequence. In essence, from some start cell, alternating activity of transition cells and place cells produced a temporally outwards propagating wave of place cell activity until a target place was found. Subsequently, backpropagation was used to find a single sequence of place cells that would be visited when travelling the shortest path from start to target. In this context, backpropagation requires a cell to know which other cell activated it, but this requirement is not biologically realistic. To alleviate this, an alternative was implemented that would stay within bounds of biological plausibility: that all learning would be online and local, for instance by using eligibility traces (Veen 2022). Eligibility traces are variables that exist internally in each neuron, and which influence the rate of learning when a learning signal is given. Typically, an eligibility trace increments when the cell activates, and decays to zero over a relatively long timespan, for instance an entire second. When a reward signal is given (for instance by finding the target during navigation), cells with a high trace-value will have activated more recently, and will be more influenced than other cells. The learning variable in this network was not weights, because the TSS model assumes that the weights from place cell to transition cell and back was learnt during exploration. Instead, the model assumes that learning occurs over the place cells’ firing delay, reducing delay of cells on the trajectory from start to target cell. The model was flexibly able to find trajectories, but it was sensitive to noise.

### A.2 Methods

In this work, a model to find place cell sequences was tested. The model was evaluated according to the stability with which a single path could be found between some arbitrary start and target cell. The requirements were that learning rules should be online and local (Veen 2022), so it could not use backpropagation, and implemented in a way that was in line with the TSS model transition cell-layer.

Place cells were first scattered across a square environment randomly and independently of each other. Each place cell had a modifiable delay between receiving an input and producing an action potential. The delay was initialized a base-delay plus a noise term. The base-delay was typically 8 ms, and the noise was uniformly distributed, for instance between 0 and 2 ms, so the place cell population would have delays uniformly distributed between 8 ms and 10 ms. In this example, noise level would be written as 25 %.

In addition to this delay, place cells would have a relatively long refractory period, higher than the maximal delay.

To determine valid transitions, a range was chosen, typically 10 cm. Any given place cell could try to activate any other place cell with receptive field centers within 10 cm of its own during the search. Comparing this to Dijkstra’s algorithm, a place cell represents nodes in a graph, and the

transition layer determines the existing edges.

Out of all place cells, two were selected - one as the start cell, the other as the target. The target neuron's delay was set to below the lowest possible initial delay, for instance 6 ms. In addition, when the goal neuron was activated, it triggered a strong inhibitory layer that would inhibit all other activity for a significant time period, typically more than the maximum delay. This inhibitory layer would activate at a significantly shorter delay than excitatory activation, for instance 1 ms after spiking.

The pathfinding model was simulated in a custom event-driven neural network, which would start by activating the start-cell. This cell would try to activate all valid place cells within its transition range. For a cell to activate, it would first have to receive such a transition signal. Then, it would activate on the condition that it was not inhibited or in a refractory period. This would work iteratively for all activated cells. Once the goal neuron was found, strong inhibition prevented all other firing across the place cell population, and the goal neuron would activate the start neuron, restarting the path search.

The learning variable was the spike delay, as well as inhibitory control. Upon receiving a learning signal, a place cell would reduce its delay significantly (equation 11)

$$d_{new} = d_{min} + (d_{old} - d_{min})/2 + \mu \quad (11)$$

Here,  $d_{old}$  and  $d_{new}$  was delay before and after learning,  $d_{min}$  was minimal delay, often 6 ms, and  $\mu$  was a noise parameter.

Next to the delay reduction, the cell would receive a tag. Tagged cells would activate the inhibitory layer in subsequent iterations, while untagged cells would not.

To receive this learning signal, the neuron tracked two internal variables. These variables could be implemented as eligibility traces which would be governed by differential equations, but in this model they were simply binary step functions. The first condition for learning was that the cell would receive an inhibitory signal shortly after firing - between 1 ms and 3 ms. The second condition was that the cell would receive a normal excitatory signal, also after firing, but at a higher delay - typically between 6 and 8 ms. Although this excitatory signal is a regular activation signal, it will in this context be understood as a 'feedback signal'.

Simulations could end in one of two ways: either because the time from start to goal would be below some fraction of the start-to-goal time in the first iteration, typically 3/4 the time, for three consecutive iterations. This would be deemed a successful simulation. Alternatively, after running for some fixed length of time, for instance a simulated second or two, the simulation would terminate in failure.

### A.3 Results

Some useful observations of the model were quickly established: first, at least with reasonable amounts of noise-levels in the initial delay, place cell activity over time resembles a travelling wave diverging from the start neuron. With low noise, this is also clearly layered in time - all the cells that are immediately activated from the start cell belong to the first layer, cells that are consecutively

activated by cells in the first layer belong to the second layer, and so forth.

The learning signal was created to encourage learning only in cells that activated a tagged cell. At the activation time of a tagged neuron, multiple cells at the forefront of the travelling wave would pass the first learning condition, receiving inhibition at the right time. However, inhibition would stop all activity for a while, so most cells would not receive any inputs. Moreover, the time window for receiving the feedback-signal was tuned to only cells with a delay below the initial minimum could provide it.

Figure A.1 shows a contour plot of this model. Each tile shows two overlaid images: the scatter plot shows all activated place cells between activation of the start cell and reaching the target. These are color-coded - start and goal are black, untagged place cells are orange and cells with a tag are colored red. The start-to-goal time is given above each tile. Underlying each scatterplot is a contour plot showing the estimated amount of simulated time it would take to get from start to any given place in the environment. This was computed with Dijkstra's algorithm over all place cells.

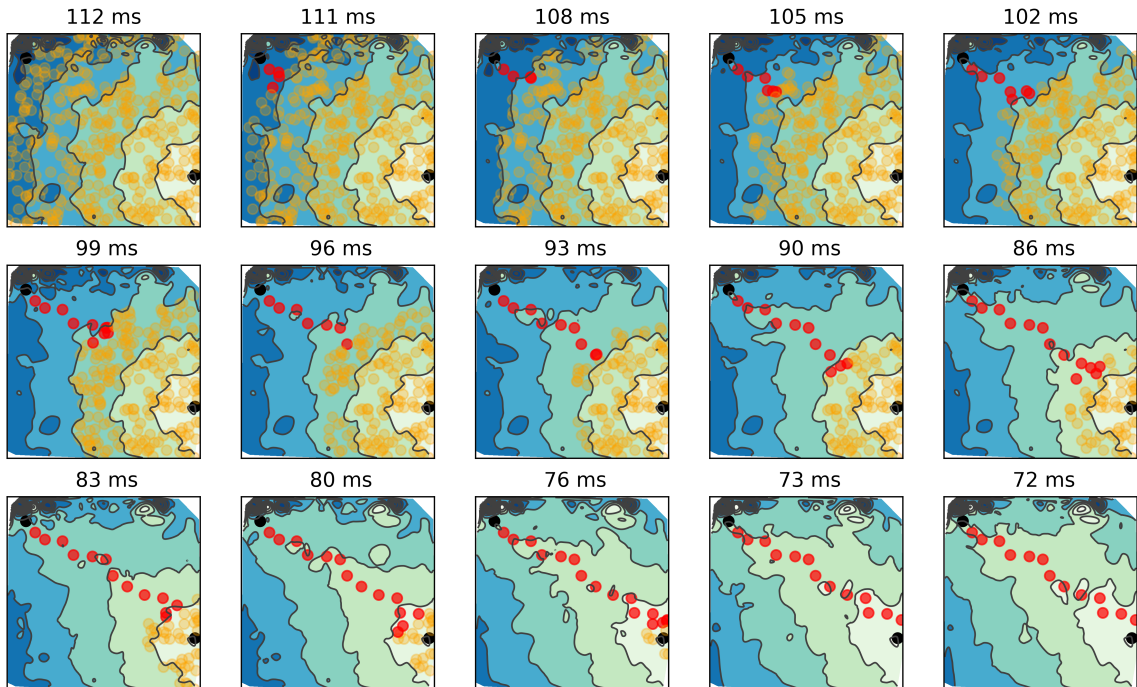


Figure A.1: Contour plot mosaic of successive iterations from start to target. Target (upper left) and start (lower right) are scatter points in black, while other place cells are colored orange if they are untagged, red if they are tagged. Only place cells that were activated during the iteration is shown. The underlying contour plot was computed with Dijkstra's algorithm from start to all place cells, in which darker colors represent longer times. Colors are the same across all plots. Each iteration takes progressively shorter times (shown above each tile), which is reflected both in the underlying contour plot and the number of successive tagged cells. This simulation passed the success-criterion with three successive iterations that were sufficiently fast relative to the first.

This reveals some features of the model: the underlying temporal landscape shown by the contour plot starts out as concentric rings, showing that the estimated time to get from start to a place is proportional to distance. In the final plots, however, time is biased in the direction from start to target. The figure also reveals a highly important reason for inhibition in this model, more than being a condition for a learning signal. More than this, the inhibitory signal removes the activation of all untagged or unnecessary cells, leaving only place cells located on the path active in the final

activation.

This can be understood by the timing dynamics of the inhibition and activation - when a tagged cell is activated, it triggers strong inhibition. Once this inhibition lifts, and all cells can fire again, the next tagged cell towards the goal will be most likely to activate because its delay is shortest.

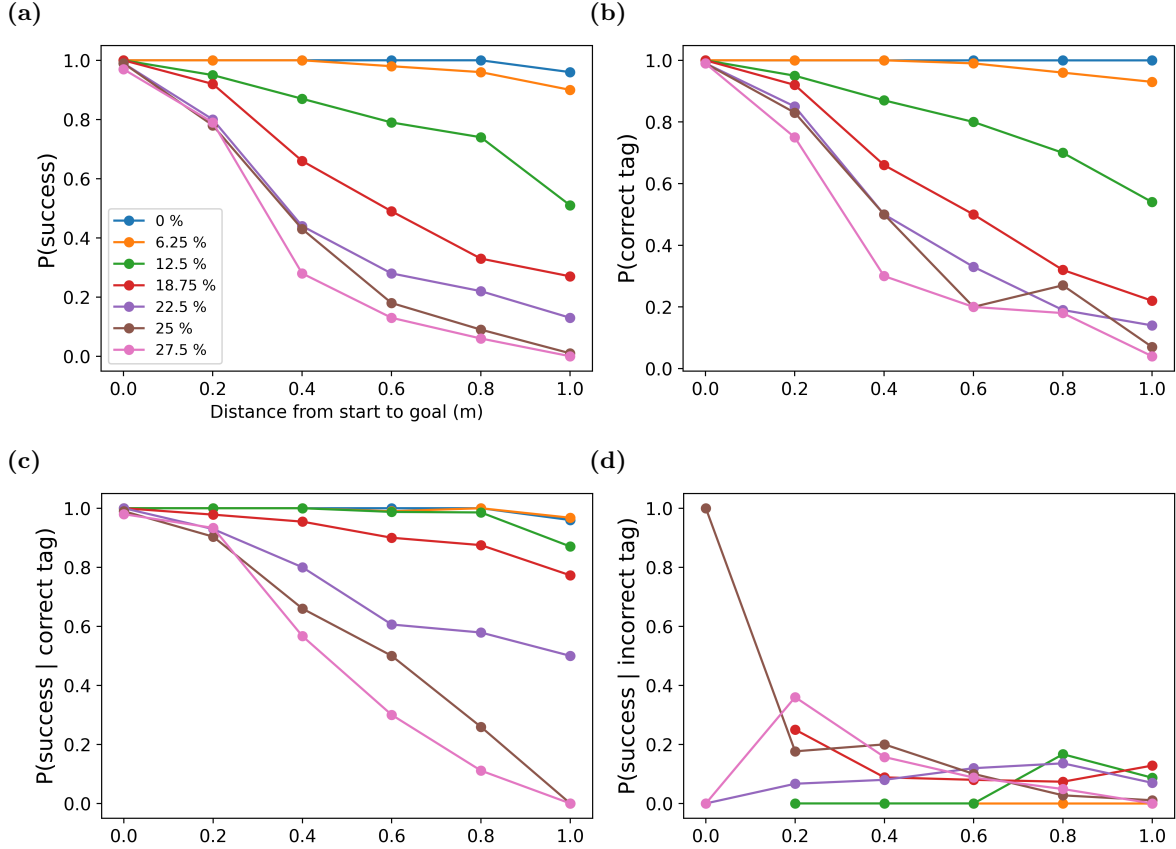


Figure A.2: Measures of success and correct tagging as a function of distance from start to goal with different levels of initial delay noise. Each point represents the mean across 100 simulations. Noise levels are shared across panels. (a & b) A simulation was deemed successful if three consecutive iterations were completed in 0.75 times the first iteration. It was correctly tagged if all tagged cells were reachable via valid transitions across tagged cells from the target cell. Success rates suffer quickly with distance already at 12.5 % noise, which is reflected in the probability in correctly tagging. (c & d) Looking only at simulations that handed out correct tags, success rates were higher, and for higher noise levels. Meanwhile, for almost all simulations, incorrectly tagging indicated low success probability regardless of distance. For the bottom two plots, notice that each point is no longer the mean of 100 - for instance, only a single simulation at 15 % noise had incorrect tag at 0 distance, which happened to be successful.

The success-rate of this model, as a function of distance from start to goal, was heavily dependent on noise in initial delay (figure A.2 (a)). Although it wasn't quantified, there were two observed reasons for the failure of this model, both influenced by this noise level. First, with this learning signal, false positives are still possible, so cells that did not activate a tagged cell still see delay reduction (figure A.2 (b)). Particularly with high levels of noise, the proportion of false positives is quite high. With high noise levels, false positives can occur because the travelling wave is less coherent, with more stray signals. Cells that activate at the right time to get the inhibitory signal might get a stray activation signal and interpret it as a correct feedback signal.

Figures A.2 (c) and (d) show the significance false positives have - simulations without false positives (figure A.2 (c)) have highly improved successrate at higher noise levels and distances.

With false positives, success rates are low regardless of noise levels and distance (figure A.2 (d))

Simulations without false positives were seen to fail when tagged cells within the same temporal layer activate each other, instead of activating a tagged cell in a next layer closer to the target. At low levels of noise, tagged cells in upcoming layers are guaranteed to have a lower delay than tagged cells in the current layer, because they have received delay-reduction more times. This is not guaranteed with high levels of noise.

Not only will this increase the time from start to target, this signal may never reach the target because it can get stuck in loops between tagged cells in the same layer. When tagged cells activate like this, they will also receive subsequent learning signals, reducing their delay and prevent activation of other cells further.

#### A.4 Discussion

Using activation delay as a learning variable is an interesting tool that arises in continuous-time networks. This has been tried in other networks (Krichmar et al. 2022; Niedermeier and Krichmar 2023), but those networks typically used Markovian transitions to simulate single paths, eventually converging on the shortest path but requiring more time. These simulations also used eligibility traces, but these were coupled with more typical reward signals upon reaching the goal, as seen in other papers (Bellec et al. 2020).

As opposed to these networks, this simulation was more reminiscent of Dijkstra's algorithm, simulating all paths in parallel (source here, and it is at least pseudo-correct to say that Dijkstra's works in parallel, right, or should I use another word?). This is more in line with the TSS model, which allows a place cell to transition to all surrounding place cells through a transition network. Importantly for this model, it was only through this transition network that place cells knew who exactly their neighbors were - neither the inhibitory signal nor the learning rules depended on proximity information beyond that given across the transition network.

Another difference between this model and previous models is that it doesn't use an eligibility trace coupled with a reward signal, but two traces. In addition, these traces weren't understood as decaying signals, but rather a signal that increased, followed by a decay.

The motivation for this temporal development of the eligibility trace is that it allowed place cells to avoid getting tagged if the learning signal arrived too soon, because in that case the learning signal couldn't have been evoked by that place cell. This shows that this model tries to solve a problem analogous to the one backpropagation tries to solve, but in a biologically plausible way: when some beneficial cell is activated, such as the target cell, which cells should be rewarded for participating in that activation? In backpropagation or backpropagation through time, this is solved by remembering all neural activations and interactions across time, so that by the time the target neuron is active, this separate memory can be used to compute the role each cell has. There is little to no evidence that the brain does this, or that a neural network can implement this separate memory structure efficiently.

Meanwhile, for the previously mentioned delay-learning simulations with Markovian activation dynamics, the reward signal released upon target-activation is sufficient because the relevance of a

given place cell is directly dependent on that place cell's activation time, so a single eligibility trace is enough to let the cell know its own role in the activation. In a travelling wave with no direction bias, the activation time is not correlated to path-relevance, making this learning rule obsolete.

A combination of these two was sought in this work. It is at most deemed a partial success, because of its struggle to converge for long distances and higher noise levels. More specifically, the role of inhibition should probably be closely scrutinized for this method to bear fruits. For this particular problem, finding a unique path across a series of connected neurons, inhibition is necessary because it is important to prevent all unwanted place cells from activating.

However, as described in the results, the dynamics here are highly dependent on precise inhibition-timing, so its fragile to noise and can end up in loops. Moreover, the double eligibility trace is missing something to guarantee convergence. In some sense, the inhibitory signal can be seen as a temporal filter, so only cells that are activated at the right time can receive the learning signal. The feedback signal can be understood as a location filter, because it is conveyed via the transition network. Both of these signals come with constraints. The inhibitory signal limits the network activity, because the network must tolerate frequent total inhibition. The feedback signal is limited because it's anonymous as a regular activation signal. This is necessary, because it move across the transition layer, which shouldn't carry information about tags or delays.

These represent problem-areas to focus on before this pathfinding model is deemed highly functional. While this work focused primarily on simulations and testing in an engineer-like fashion, advanced can probably be made with more theoretical and mathematical considerations. Following ideas from TSS, it would also be interesting to implement transitions on multiple scales, for instance by reflexively increasing scale after a given number of transitions.